

pubs.acs.org/estair Article

Applying a Phase-Separation Parameterization in Modeling Secondary Organic Aerosol Formation from Acid-Driven Reactive Uptake of Isoprene Epoxydiols under Humid Conditions

Yuzhi Chen, Alexandra E. Ng, Jaime Green, Yue Zhang, Matthieu Riva, Theran P. Riedel, Havala O. T. Pye, Ziying Lei, Nicole E. Olson, Madeline E. Cooke, Zhenfa Zhang, William Vizuete, Avram Gold, Barbara J. Turpin, Andrew P. Ault, and Jason D. Surratt*



Cite This: https://doi.org/10.1021/acsestair.4c00002



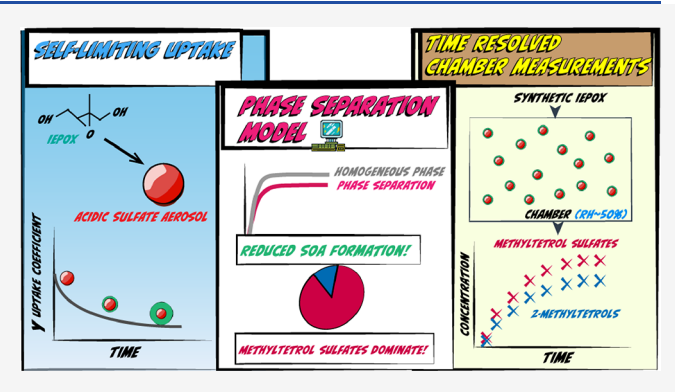
ACCESS

III Metrics & More

Article Recommendations

Supporting Information

ABSTRACT: Secondary organic aerosol (SOA) from acid-driven reactive uptake of isoprene epoxydiols (IEPOX) contributes up to 40% of organic aerosol (OA) mass in fine particulate matter. Previous work showed that IEPOX substantially converts particulate inorganic sulfates to surface-active organosulfates (OSs). This decreases aerosol acidity and creates a viscous organic-rich shell that poses as a diffusion barrier, inhibiting additional reactive uptake of IEPOX. To account for this "self-limiting" effect, we developed a phase-separation box model to evaluate parametrizations of IEPOX reactive uptake against time-resolved chamber measurements of IEPOX SOA tracers, including 2-methyltetrols (2-MT) and methyltetrol sulfates (MTS), at ~50% relative humidity. The phase-separation model was most sensitive



to the mass accommodation coefficient, IEPOX diffusivity in the organic shell, and ratio of the third-order reaction rate constants forming 2-MT and MTS ($k_{\rm MT}/k_{\rm MTS}$). In particular, $k_{\rm MT}/k_{\rm MTS}$ had to be lower than 0.1 to bring model predictions of 2-MT and MTS into closer agreement with chamber measurements; prior studies reported values larger than 0.71. The model-derived rate constants favor more particulate MTS formation due to 2-MT likely off-gassing at ambient-relevant OA loadings. Incorporating this parametrization into chemical transport models is expected to predict lower IEPOX SOA mass and volatility due to the predominance of OSs.

KEYWORDS: multiphase chemistry, box modeling, core-shell morphology, rate constants, diffusion limitation

INTRODUCTION

Isoprene (2-methyl-1,3-butadiene, C_5H_8) is the most abundant reactive non-methane volatile organic compound (VOC) and mainly emitted from vegetation into the atmosphere, with annual emissions estimated from 500 to 750 Tg.^{2,3} Atmospheric oxidation of isoprene by hydroxyl radicals (*OH) is its dominant sink (~85% on average globally). 4,5 The initial attack of OH on isoprene occurs predominantly at either C_1 (0.63) or C_4 (0.37) due to the formation of resonance-stabilized allylic radicals. Molecular oxygen (O2) quickly adds to the allylic radicals, forming isoprene hydroperoxyl radicals (ISOPOO*). The atmospheric fate of ISOPOO determines the subsequent reaction pathways and secondary organic aerosol (SOA) formation potential.⁷⁻⁹ When nitric oxide (NO) levels are low (i.e., <1 ppb), ISOPOO primarily reacts with hydroperoxyl radicals (HO2*), which yields predominantly (~90%) isoprene hydroxyhydroperoxides (ISOPOOH). 4,10,11

Major products following *OH addition to ISOPOOH are isomeric isoprene epoxydiols (IEPOX) with a yield of ~70–

80%.^{11–13} IEPOX has also been identified from the *OH-initiated oxidation of isoprene under high-NO conditions, although the yield is much lower (i.e., 13% from parent hydroxynitrates) than that from ISOPOOH under high-NO conditions.¹⁴ When gaseous IEPOX is taken up by inorganic sulfate (Sulf_{inorg}, which is composed of both HSO₄⁻ and SO₄²⁻) aerosol, it can undergo acid-enhanced reactions and yield a wide array of compounds including polyols, low-volatility organosulfates (OSs), and oligomers that contribute to SOA mass.^{15–18} This process is termed IEPOX heterogeneous or multiphase chemistry. The most abundant SOA constituents resulting from IEPOX multiphase chemistry are 2-methyltetrols (2-MT) and

Received: January 5, 2024 Revised: April 4, 2024 Accepted: April 4, 2024



methyltetrol sulfates (MTS or IEPOX OS). 16,17,19 2-Methyltetrol sulfate (2-MTS) diastereomers have been recently demonstrated to be the dominant isomers of MTS. 19 MTS have been recently measured to contribute up to 13% of the organic carbon (OC) in fine particulate matter (PM_{2.5}) collected from downtown Atlanta²⁰ and Look Rock, Tennessee, U.S., ¹⁹ up to 10% of the total organic matter (OM) mass in PM_{2.5} collected downwind of Manaus, Brazil,²¹ and up to 15% of the total OM mass in PM_{2.5} collected during the 2017 Lake Michigan Ozone Study (LMOS).²² MTS and their corresponding oligomers may help explain the low-volatility nature of IEPOX SOA^{23,24} and the substantial contribution of IEPOX SOA (30-40%) toward the fine OA mass measured in many isoprene-rich locations. 18,23,25,26 Due to high abundance of IEPOX SOA within ambient PM_{2.5}, it is critical to understand the formation mechanisms, physicochemical properties, and potential atmospheric fates of its low-volatility OSs.

Key components required for SOA formation from IEPOX include aerosol liquid water, proton donors (e.g., H⁺ or NH₄⁺) for ring-opening reactions of IEPOX, and nucleophiles (e.g., H₂O, SO₄²⁻, NO₃⁻, and preexisting 2-MT and MTS) to promote further condensed-phase reactions leading to the formation of IEPOX SOA components. The kinetics of IEPOX reactive uptake are different from the equilibrium partitioning theory that is based on Raoult's law. Instead, the reactive uptake of IEPOX depends on the solubility of IEPOX (determined by an effective Henry's law coefficient), aerosol-phase acidity, and condensed-phase nucleophilic reactivity. 27-30 Taking these factors into account, both regional- and global-scale chemical transport models represent the multiphase chemistry of IEPOX, assuming a homogeneous aerosol phase through a reactive uptake coefficient (γ_{IEPOX}) derived using a resistor model.^{31–3} Using a semi-explicit treatment of IEPOX reactive uptake, improvements have been made in closing the gap between simulations and observations.^{31,38-41} However, large errors in model performance, as well as high sensitivity towards and uncertainty in key parameters associated with such an approach, still persist, suggesting a need for constraining parameters such as the Henry's law constants of IEPOX and aerosol-phase reaction rate constants. 38,41,42

2-MT and MTS together contribute a major mass fraction (>90% at Look Rock, Tennessee, U.S.) of IEPOX-derived SOA.¹⁹ In regulatory models, the third-order reaction rate constants forming these two monomer species (see reactions R2 and R3, described in the next section) were typically obtained from kinetic measurements in bulk solution. 27,28 Given the differences in pK_a values between $Sulf_{inorg}$ and OSs, rapid inorganic-to-organic sulfate conversion by IEPOX, as shown in our recent chamber studies, reduces the acidity of the aqueous phase. 18,34,43,44 In addition, the substantial formation of surfaceactive OSs results in an aerosol morphology that has a viscous organic-rich shell surrounding an aqueous inorganic core with decreasing acidity. 18,34,43,44 The viscous organic shell increases the diffusional barrier that IEPOX must overcome to reach the aqueous core, slowing down the overall reaction. 18,34 Consequently, acid-driven reactive uptake of IEPOX is inhibited by the changes in aerosol acidity and phase state induced by this multiphase chemistry over time. 18,

The preexisting organic coating has been considered in modeling IEPOX multiphase chemistry previously, ^{36,37,45} and recently, this so-called "self-limiting" effect was considered in modeling chamber experiments (e.g., Octaviani et al. ⁴⁶ under dry conditions and Zhang et al. ⁴⁷ under humid conditions).

However, these studies lack direct and real-time measurements of critical IEPOX SOA tracers, including 2-MT and MTS, which are needed to constrain the models.

In this work, we investigate IEPOX reactive uptake under humid conditions (relative humidity (RH) $\sim 50\%$) using a zero-dimensional box model that considers the self-limiting effect of IEPOX SOA formation and is constrained by key tracers. The time-resolved chemical measurements of IEPOX SOA molecular tracers from the UNC chamber experiments provide a unique opportunity to evaluate and refine the phase-separation model and parameters so that they reproduce the key chemical features of IEPOX SOA evolution. We provide insights into parameters that have the largest impact on the time evolution of the IEPOX SOA tracers in the chamber through sensitivity analysis. We then apply the model to simulate hypothetical atmospherically relevant scenarios to show the importance of considering phase separation in the atmospheric formation of IEPOX SOA.

EXPERIMENTAL SECTION

Smog Chamber Experiments. Measurements for model evaluation are obtained from IEPOX reactive uptake experiments conducted in the UNC indoor environmental chamber facility with $trans-\beta$ -IEPOX and acidified ammonium sulfate seed aerosol (AAS) under humid conditions (RH ~ 50%). These include published experiments 18,43 and new experiments (Table S1). While the seed type and initial acidity were kept constant, the relative amounts of injected trans-β-IEPOX and Sulf_{inorg} concentration were varied between experiments to represent a range of atmospherically relevant IEPOX:Sulf_{inorg} ratios. 18 The time-resolved Sulf_{inorg} (HSO₄⁻ + SO₄²⁻) and organic tracers, including 2-MT and 2-MTS, were obtained by measurements coupling online collection using a particle-intoliquid sampler (PILS) to offline chemical analyses by ion chromatography (IC) and ultra performance liquid chromatography interfaced to electrospray ionization high-resolution quadrupole-time-of-flight mass spectrometry (UPLC/ESI-HR-QTOFMS). The total dry aerosol volume concentration and size distribution were constantly monitored in real time by a scanning electrical mobility sizer (SEMS, Brechtel, Inc.) and used to derive total dry SOA volume concentrations (Section S2.1). The experimental setup, online sample collection, and offline chemical analyses have been detailed previously 18,43 (also see Section S1). Note that the IEPOX SOA tracer measurements using these methods have an uncertainty of 14-17% (RSD), as determined in our previous work. 18,19,43,48 Therefore, a deviation within ±25% of the measurements is considered a reasonable model performance in the current study.

Box Model Setup. We investigated the reaction kinetics of IEPOX SOA formation using a zero-dimensional time-dependent chemical reaction kinetics box model. Like our prior work, the box model simulates gas-phase IEPOX uptake by Sulf_{inorg} aerosol and includes semi-explicit aerosol-phase tracer formation (reactions R1–R5, described below). Updates were made in line with the latest understanding of the reaction products, resulting aerosol physicochemical properties, and feedback on IEPOX uptake. Specifically, recent studies have demonstrated that C₅-alkene triols and 3-methyltetrahydrofuran-3,4-diols (3-MeTHF-3,4-diols) are not thermodynamically feasible products from IEPOX isomerization and are likely degradation products of IEPOX-derived OSs and oligomers formed because of heated vaporization/ionization methods and/or trimethylsilylation for sample pretreament. 19,49–S1

Therefore, reactions forming the diols and triols were removed in the model, but reactions leading to the formation of 2-MT, MTS, and their respective dimers were kept, as shown in reactions R2–R5. The reaction rate constants we used, along with literature values, are summarized in Table S2. We assumed that reaction product monomers only form in the aqueous core (reactions R2 and R3) and immediately salt-out to the aerosol particle surface (shell), as demonstrated by recent measurements. R3,34 Oligomers are assumed to form only in the organic shell from monomers (reactions R4 and R5). 2-MT is treated as semivolatile with a saturation vapor pressure (C^*) of 8.31 μ g m⁻³. The particle-phase fraction of 2-MT was calculated as shown in eq 1, where C_{OA} is the mass concentration of total SOA.

$$IEPOX(g) \xrightarrow{k_{het}} IEPOX(aq)$$
 (R1)

IEPOX(aq) + H⁺ + H₂O
$$\xrightarrow{k_{H^{+},H_{2}O}} 2$$
-MT + H⁺ (R2)

IEPOX(aq) + H⁺ +
$$SO_4^{2-} \xrightarrow{k_H t, SO_4^{2-}} MTS$$
 (R3)

IEPOX(aq) + H⁺ + 2-MT
$$\xrightarrow{k_{\text{H}^{+},2-\text{MT}}}$$
 2-MT dimer + H⁺
(R4)

IEPOX(aq) + H⁺ + MTS
$$\xrightarrow{k_{\text{H}^{+},\text{MTS}}}$$
 MTS dimer + H⁺
(R5)

$$F_{\rm p} = \frac{\rm particle}{\rm gas + particle} = \left(1 + \frac{C^*}{C_{\rm OA}}\right)^{-1} \tag{1}$$

The time-dependent pseudo-first-order heterogeneous reaction rate constant $(k_{\text{het}}(t), \text{ s}^{-1})$ of IEPOX with $\text{Sulf}_{\text{inorg}}$ aerosol is calculated by eq 2:

$$k_{\text{het}}(t) = \frac{\gamma_{\text{IEPOX}}(t)S_{\text{a}}(t)\omega}{4}$$
 (2)

where $\gamma_{\rm IEPOX}(t)$ is the IEPOX(g)—aerosol reaction probability or reactive uptake coefficient, ω (cm s⁻¹) is the mean molecular speed of IEPOX vapor, and $S_{\rm a}(t)$ is the total aerosol surface area concentration (cm² cm⁻³).

The main difference between the modeling approach here and that of our previous work is the treatment of $\gamma_{\rm IEPOX}$, where the self-limiting effect is embedded. Instead of using a constant value derived from flow tube measurements, 32 $\gamma_{\rm IEPOX}(t)$ is treated as a time-dependent parameter and calculated using a resistor model (eq 3): 46,53

$$\frac{1}{\gamma_{\text{IEPOX}}(t)} = \frac{r_{\text{p}}(t)\omega}{4D_{\text{g}}} + \frac{1}{\alpha} + \frac{r_{\text{p}}(t)\omega}{4RTH_{\text{org}}D_{\text{org}}(q_{\text{org}}F - 1)}$$
(3)

where $r_{\rm p}(t)$ is the aerosol particle radius, $D_{\rm g}$ (cm² s⁻¹) is the diffusion coefficient of IEPOX in the gas phase, α is the mass accommodation coefficient, R is the ideal gas constant (L atm K⁻¹ mol⁻¹), and T is the temperature (K). $H_{\rm org}$ is the Henry's law constant of IEPOX in the organic shell, set to 2.0×10^6 M atm⁻¹ based on prior studies. 46,54 $D_{\rm org}$ (cm² s⁻¹) is the diffusivity of IEPOX in the phase-separated organic shell. While $D_{\rm org}$ is tied to the chemical composition of the organic shell, it was set to a constant value in the current model and evaluated in sensitivity runs (see the Sensitivity Analysis Results section). The functions F(t) and $q_{\rm org}(t)$ are calculated as eqs 4–8:

$$F(t) = \frac{\coth(q_{\text{org}}(t)) + h(q_{\text{aq}}(t), q_{\text{org}}^{*}(t))}{1 + \coth(q_{\text{org}}(t))h(q_{\text{aq}}(t), q_{\text{org}}^{*}(t))}$$
(4)

 $h\Big(\,q_{ag}^{}(\,t\,)\,,q_{org}^{\,*}(\,t\,)\,\Big) = \,-\tanh\!\Big(\,q_{org}^{\,*}\Big)\,\cdot$

$$\left[\frac{\frac{H_{aq}D_{aq}}{H_{org}D_{org}}\left(q_{aq}(t)\coth\left(q_{aq}(t)\right)-1\right)-\left(q_{org}^{*}(t)\coth\left(q_{org}^{*}(t)\right)-1\right)}{\frac{H_{aq}D_{aq}}{H_{org}D_{org}}\left(q_{aq}(t)\coth\left(q_{aq}(t)\right)-1\right)-\left(q_{org}^{*}(t)\tanh\left(q_{org}^{*}(t)\right)-1\right)}\right] (5)$$

$$q_{\text{org}}^{*}(t) = \frac{r_{\text{c}}(t)}{r_{\text{p}}(t)} q_{\text{org}}(t)$$
(6)

$$q_{\rm aq}(t) = r_{\rm c}(t) \sqrt{\frac{k_{\rm aq}(t)}{D_{\rm aq}}}$$
(7)

$$q_{\text{org}}(t) = r_{\text{p}}(t) \sqrt{\frac{k_{\text{org}}(t)}{D_{\text{org}}}}$$
(8)

where $H_{\rm aq}$ (1.7 × 10⁸ M atm⁻¹)³¹ and $D_{\rm aq}$ (1 × 10⁻⁵ cm² s⁻¹)⁵⁵ are the Henry's law constant and diffusion coefficient for IEPOX dissolution into the inorganic aqueous core, respectively, $r_{\rm c}(t)$ is the radius of the inorganic aqueous core, and $k_{\rm aq}(t)$ and $k_{\rm org}(t)$ are the sum of first-order reaction rates (s⁻¹) in the aqueous core and the organic shell, expressed as eqs 9 and 10, respectively:

$$k_{aq}(t) = \sum_{i=1}^{N} k_i [\text{nuc}_i(t)] [aH_{aq}^{+}]$$
(9)

$$k_{\text{org}}(t) = \sum_{i=1}^{M} k_i [\text{nuc}_i(t)] [aH_{\text{shell}}^{\dagger}]$$
(10)

Here, $[aH_{aq}^{+}]$ is the hydrogen ion activity in the aqueous core, calculated as the product of the H⁺ activity coefficient $(\gamma_{H^{+}})$ and the H⁺ concentration in the aqueous core $([H_{aq}^{+}])$. Initial $[H_{aq}^{+}]$ is output from E-AIM. $[aH_{shell}^{+}]$ is the hydrogen ion activity in the organic shell. $[aH_{shell}^{+}]$ is set to $1/100[aH_{aq}^{+}]$ to reflect the relative lower acidity in the shell based on our previous modeling. 34 [nuc $_i$] is the time-dependent concentration of the ith nucleophile, and k_i is its corresponding third-order reaction rate constant in each phase. Note that the acidity at aerosol interfaces, including the aerosol–gas interface and internal interface (core–shell), is uncertain and has suggested results ranging from more 56 to less acidic. 57 Experimental data are needed to confidently relate the pH in the core to the shell and surface/interface enhancements.

The time-dependent total surface area concentration $(S_a(t))$, inorganic core radius $(r_c(t))$, and aerosol radius $(r_p(t))$ are derived from the net volume (V(t)) change calculated using simulated dry SOA mass and $\mathrm{Sulf}_{\mathrm{inorg}}$ with proper conversion using hygroscopic growth parameters and densities associated with the organic and inorganic fractions, respectively. It is important to note that the model treats the aerosol population as monodisperse, initiated from the measured mode diameter of the seed aerosol. The detailed calculations regarding the aerosol size dynamics are described in Section S2.1.

The model is initialized with the amount of $trans-\beta$ -IEPOX added to the injection manifold, initial seed aerosol volume concentration, surface area concentration, and ionic chemical composition. The initial molar concentrations of inorganic seed aerosol species ([NH₄⁺], [H⁺], [H₂O], [HSO₄⁻], and [SO₄²⁻])

Table 1. Values of Model Parameters for Base Simulation and Sensitivity Analysis Cases

name	parameter	base	equation	low	high			
IEPOX gas-phase diffusion coefficient	$D_{\rm g}~({\rm cm^2~s^{-1}})$	eq	$D_{\rm g} = 1.9 ({\rm MW_{\rm IEPOX}})^{-2/3}_{36}$	-	-			
IEPOX mean molecular speed	ω (cm s ⁻¹)	eq	$\omega = \sqrt{\frac{8RT}{\pi MW^{36}}}$	-	-			
Sensitivity								
mass accommodation coefficient	α	$0.02^{38,39}$	-	0.001^{47}	0.1^{31}			
activity coefficient of H ⁺	$\gamma_{ ext{H}^{^+}}$	1	-	_	8			
Henry's law constant of the aqueous phase (core)	H_{aq} (M atm ⁻¹)	1.7×10^{831}	-	3×10^{776}	4×10^{831}			
Henry's law constant of the organic phase (shell)	H_{org} (M atm ⁻¹)	2×10^{633}	-	-	-			
IEPOX organic-phase diffusion coefficient	$D_{\rm org} ({\rm cm}^2 {\rm s}^{-1})$	2×10^{-12}	-	2×10^{-13}	2×10^{-11}			
ratio of third-order reaction rate constant of IEPOX with water and $\mathrm{SO_4}^{2-}$	$k_{ m MT}/k_{ m MTS}$	0.11	-	0.05	0.2			

and total aqueous aerosol-phase volume are obtained from the Extended AIM Aerosol Thermodynamic Model II (E-AIM, http://www.aim.env.uea.ac.uk/aim/aim.php)^{58,59} by inputting the initial moles of SO_4^{2-} , NH_4^+ , and H^+ in the chamber. The molarities of the ions were calculated from Sulf_{inorg} obtained by IC, assuming a 1:1:1 ratio since equal molarities of ammonium sulfate $((NH_4)_2SO_4)$ and sulfuric acid (H_2SO_4) were combined to make the atomizer solution. Measured temperature (K) and RH (%) were averaged over the 1 h IEPOX injection time and input into E-AIM as well (Table S1). The rate at which IEPOX was injected into the chamber was assumed a first-order decay of IEPOX in the injection manifold. The decay rate constant derived was varied between 1.2×10^{-4} and 2.4×10^{-4} s⁻¹ as a fitting parameter to match the injection efficiency calculated from the manifold weight determined gravimetrically before and after injection for each experiment. First-order gas wall-loss rates estimated from published experiments^{29,32} are applied to gasphase IEPOX ($k_{\text{wall-IEPOX}} = 9.45 \times 10^{-5} \,\text{s}^{-1}$). Experiment-specific first-order aerosol wall-loss rates were estimated from the seed only period of each experiment and applied to all aerosol-phase species $(k_{\text{wall-aerosol}} = 1 \times 10^{-5} - 1 \times 10^{-4} \text{ s}^{-1})$. The coupled ordinary differential equations (ODEs) corresponding to the production and/or loss of all gas- and aerosol-phase species were solved and integrated over the 1 h duration of IEPOX injection in MATLAB (R2019a). Key differences between the current phase-separation model and previous studies are summarized in Section S3.

Model Evaluation. Model parameters and their values used in the base case simulation are summarized in Table 1. Note that the core—shell model holds parameters constant throughout the course of the 1 h reactive uptake experiment. These parameters include the following: $[H^+]$, γ_{H^+} , HSO_4^-/SO_4^{2-} ratio, D_{org} and H_a . We used normalized mean bias (NMB) to describe the model performance for concentrations of the three key aerosolphase species that have time-resolved measurements: 2-MT, MTS, and $Sulf_{inorg}$. The equation to calculate NMB is as follows:

$$NMB_{i} = \frac{\sum_{m=1}^{n} (M_{i,m} - O_{i,m})}{\sum_{m=1}^{n} O_{i,m}}$$
(11)

where $M_{i,m}$ and $O_{i,m}$ are the *m*th modeled and observed concentrations, respectively, of the *i*th SOA species.

To identify the model parameters to which outputs are most sensitive, an analysis was performed that included α , $\gamma_{\rm H}$, $H_{\rm a}$, $D_{\rm org}$ and the ratio of the third-order rate constants of reactions forming 2-MT and MTS ($k_{\rm MT}/k_{\rm MTS}\sim0.1$). The parameter values for the sensitivity analysis are summarized in Table 1.

RESULTS AND DISCUSSION

Core—**Shell Model Base Case Performance.** NMB values for the base case are reported in Table 2 and include all model

Table 2. Normalized Mean Bias (NMB) of Simulated Key Aerosol-Phase Species in All Sensitivity Scenarios

case	$Sulf_{inorg}$	2-MT	MTS	2-MT/MTS
base	0.04	0.58	0.14	0.16
low accom	0.15	-0.31	-0.46	0.07
high accom	0.03	0.66	0.19	0.16
high $\gamma_{ ext{H}^+}$	0.03	0.64	0.18	0.16
$low H_a$	0.07	0.28	-0.06	0.13
high $H_{ m a}$	0.03	0.62	0.16	0.16
${\rm low}\ D_{\rm org}$	0.08	0.23	-0.08	0.12
high D_{org}	0.03	0.66	0.18	0.17
low $k_{\text{MT/MTS}}$	0.01	-0.12	0.27	0.01
high $k_{ m MT/MTS}$	0.07	1.55	-0.04	0.38

runs with timestamps up to $\sim\!1$ h for all nine experiments (Table S1). The best "base case" prediction is for Sulf_{inorg}, which had a near-zero NMB (0.04). 2-MT is extensively overpredicted in the base case (NMB of 0.58). MTS is slightly overpredicted (NMB of 0.14). The NMB for individual experiments (Table S3), however, reveals that model performance varied depending on the initial IEPOX:Sulf_{inorg}. As IEPOX:Sulf_{inorg} increases, the base case parameterization leads to a greater overprediction of Sulf_{inorg} and MTS (Figure 1 and Table S3). Overall, 2-MT is the most poorly predicted IEPOX SOA tracer with the base case parameterization.

Compared to prior studies that obtained chemical speciation data only from filter samples at the SOA growth end point, 29,46,47 the PILS-IC and PILS-UPLC/ESI-HR-QTOFMS measurements in the present work are advantageous in providing time-resolved chemical speciation. This allows model performance assessment of not only the total SOA formed but also the dynamic evolution of individual inorganic and organic aerosol species. For a time series evaluation, we selected two experiments with IEPOX:Sulfinorg values at the extreme ends of the atmospherically relevant range, 18 which included experiment 5 (Expt. 5) (IEPOX:Sulf_{inorg} = 1.0) and Expt. 3 (IEPOX:Sulf_{inorg} = 10.2). We observed that the base case parameterization was marginally better at reproducing 2-MT but worse at reproducing particulate sulfur containing species (Sulf_{inorg} and MTS) in high IEPOX:Sulf_{inorg} conditions (Expt. 3) than in low IEPOX:Sulf_{inorg} conditions (Expt. 5) (Table S3). Measured data show that in Figure 2A (Expt. 3 (high IEPOX:Sulf_{inorg})), comparable particulate mass concentrations

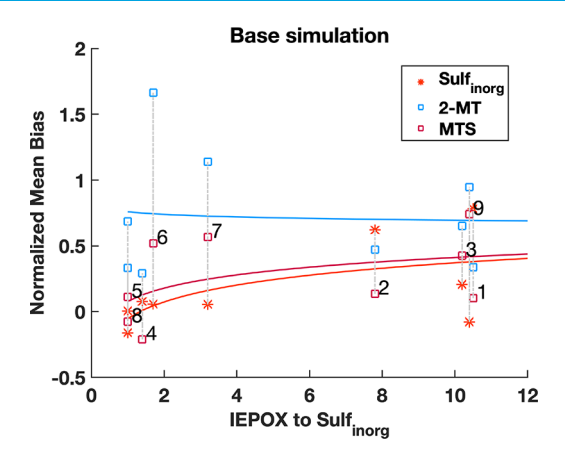


Figure 1. Calculated normalized mean bias (NMB) values of modeled particulate species, including inorganic sulfate (Sulf_{inorg}), 2-methyltetrols (2-MT), and methyltetrol sulfates (MTS), as a function of the IEPOX:Sulf_{inorg} ratio. The three lines whose colors correspond to the three particulate species are logarithmic fits of the observations to visualize the trends. The numbers next to the MTS data points correspond to the experiment index in Table S1. Each vertical dashed line connects the data points for Sulf_{inorg}, 2-MT, and MTS from the same experiment.

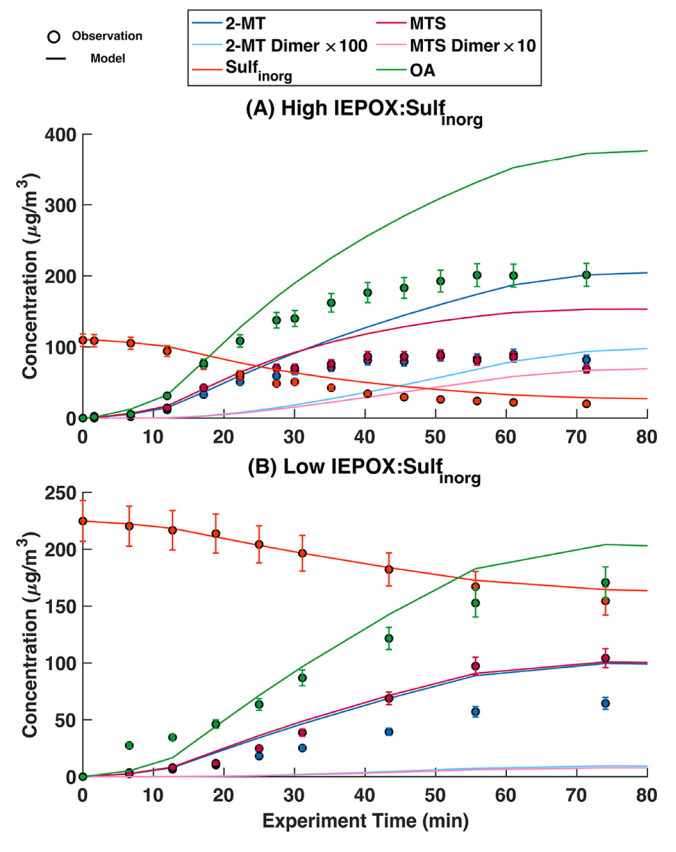


Figure 2. Base simulation of IEPOX SOA tracers and total SOA for (A) high IEPOX:Sulf_{inorg} ratio experiment (Expt. 3, Table S1) and (B) low IEPOX:Sulf_{inorg} ratio experiment (Expt. 5, Table S1). Observations are shown as shaded circles with error bars (1σ) , and simulations are shown as solid lines. Color codes are displayed in the legend.

of 2-MT and MTS were formed rapidly during the first 30 min, but the formation rates leveled off during the second 30 min. The base case parameterization overpredicts the rates of production of both particulate 2-MT and MTS after 20 min.

MTS was more reasonably predicted than 2-MT. In Expt. 5 (Figure 2B, low IEPOX:Sulf_{inorg}), measured particulate-phase formation of the two monomers did not significantly slow until $\sim\!50$ min. The low IEPOX:Sulf_{inorg} value explains the increased formation of MTS relative to 2-MT (Figure 2B). The base case parameterization produced similar amounts of both tracers, leading to an overprediction of particulate 2-MT throughout the entire hour. Overall, these differences in the evolution of particulate 2-MT and MTS that are dependent on IEPOX:Sulf_{inorg} were not reproduced well by the base case parameterization.

Sensitivity Analysis Results. The NMB for each sensitivity case for each particulate species was calculated, and the values are summarized in Table 2. When compared to the base case parametrization, the model performance (NMBs and the normalized biases for individual data points) barely changed in the Low H_a and High H_a cases even though the H_a values span over an order of magnitude (Table 2 and Figure 3). The same conclusion can be drawn from a close inspection of the NMBs shown in Table S4 and Figures S2-S4. This confirms that the dissolution of IEPOX in the aqueous core is not the limiting factor in the core—shell treatment. Higher γ_{H^+} (8) resulted in small increases in the production of all SOA, leading to a slightly worse agreement for the two IEPOX SOA tracers (Table 2 and Figures 3 and S2B). More distinguishable differences in the model outputs were found for the Mass Accom, D_{org} , and $k_{\rm MT/MTS}$ sensitivity cases, which we discuss in detail in the following sections. It should be noted that the NMB for each sensitivity run is intended to resolve the magnitude of change in response to varying values of model parameters. Since only one parameter was varied at a time with the others held constant (at base case values), the value that resulted in the best model performance in the sensitivity run does not necessarily lead to the same model performance if other parameters were also

Mass Accommodation Coefficient (α). α is commonly defined as the probability of a gas molecule entering the aerosol per collision with the aerosol surface. 60 It should be noted that α here is more of a traditional definition of mass accommodation. It does not clearly distinguish gas-surface and surface-bulk mass transport like later developed multilayer kinetic model frameworks 61-63 and molecular dynamics simulations. 64,65 Therefore, it should not be confused with the surface accommodation coefficient $(\alpha_{\rm s})$ under these frameworks. It should also not be confused with the effective mass accommodation coefficient $(lpha_{ ext{eff}})$ recently proposed by Shiraiwa and Pöschl, which accounts for diffusivity and reactivity within the penetration depth in representing α_s . ⁶⁶ Furthermore, Kolb et al. summarized the terminologies used in gas uptake studies and different definitions for the mass accommodation coefficient used in different experimental and simulation approaches that could lead to discrepancies when comparing values. 67

In the resistor representation, the mass accommodation coefficient sets the baseline resistance $(1/\alpha)$ (eq 3). The base case value (α = 0.02) was commonly used in several modeling studies. ^{29,35,38,39,46} We chose 0.02 here, as it best reproduces the initial γ for IEPOX uptake onto acidified sulfate seed determined from our previous flow tube measurement. ³² A higher value (α = 0.1) suggested by Gaston et al. ³¹ was selected for the High Accom case. The Low Accom case value (α = 0.001) was suggested by Zhang et al., ⁴⁷ as it better captures the IEPOX SOA growth at the beginning of their experiments. In our simulations, the higher mass accommodation coefficient (α = 0.1) slightly

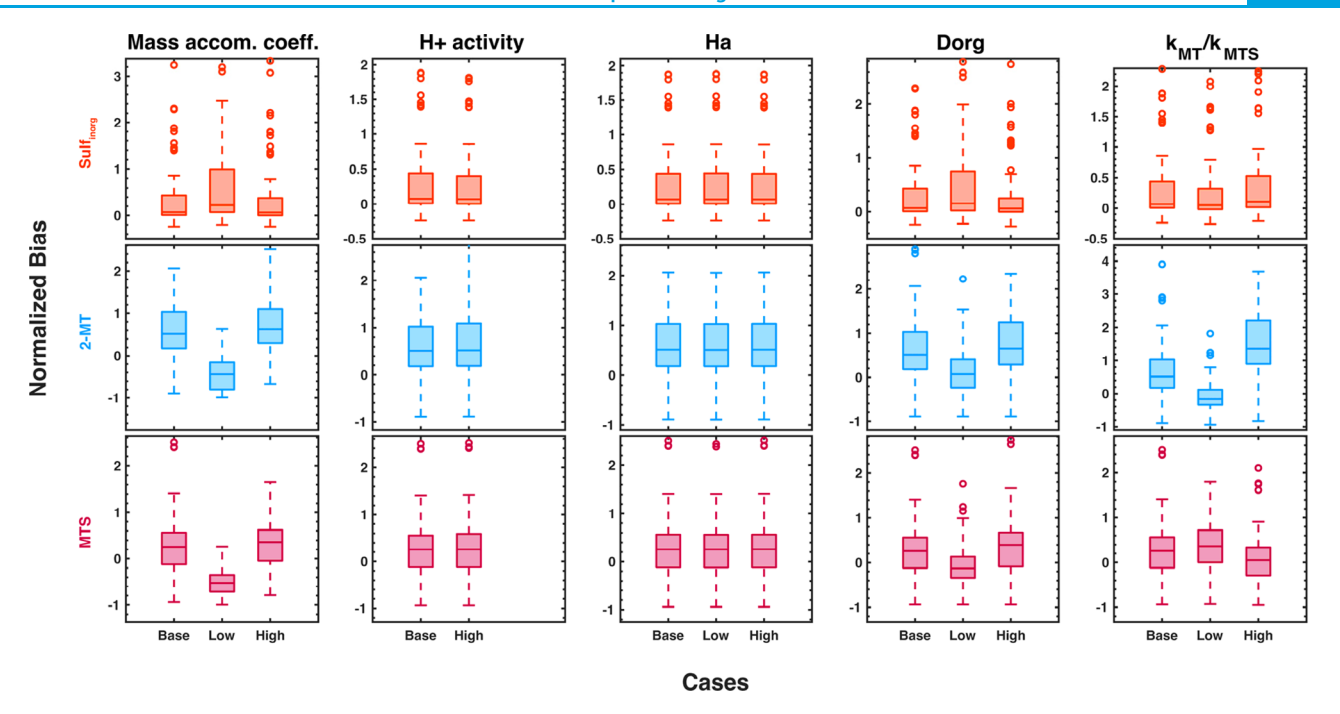


Figure 3. Box plots of NMBs of individual modeled Sulf_{inorg} (orange), 2-MT (blue), and MTS (burgundy) for all five model sensitivity scenarios. In each box, the central mark indicates the median, and the bottom and top edges of the box indicate q_1 (25th percentile) and q_3 (75th percentile), respectively. The whiskers extend to the most extreme data points not assigned as outliers. The data points are considered outliers if they are greater than $q_3 + 1.5(q_3 - q_1)$ or less than $q_1 - 1.5(q_3 - q_1)$. The outliers are shown individually with open circles.

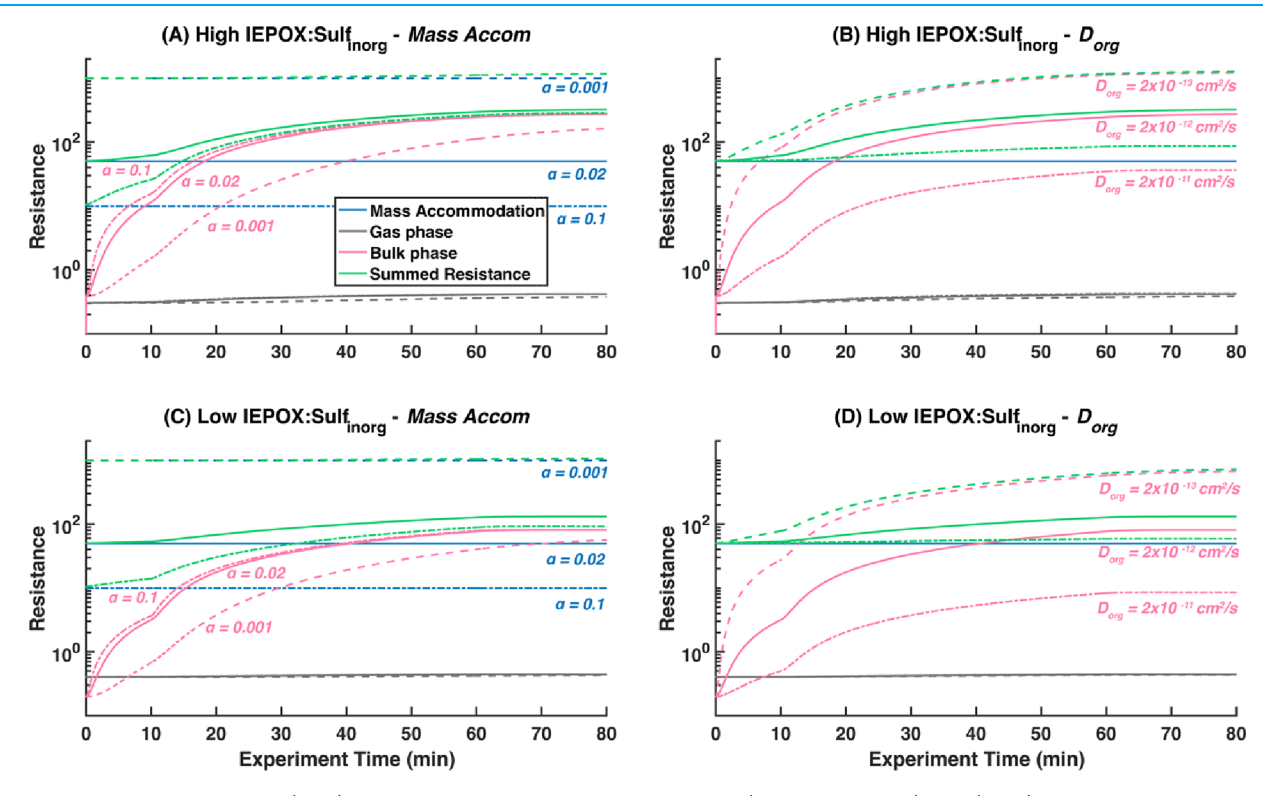


Figure 4. Simulated resistance for (A, B) the high IEPOX:Sulf_{inorg} ratio experiment (Expt. 3, Table S1) and (C, D) the low IEPOX:Sulf_{inorg} ratio experiment (Expt. 5, Table S1). Dark gray curves are resistance from gas-phase diffusion (first term in eq 3). Blue curves are resistance from mass accommodation (second term in eq 3). Pink curves are resistance from the bulk phase (third term in eq 3). Green curves are the overall resistance, summing up all three resistor terms $(1/\gamma_{\text{IEPOX}})$. (A) and (C) are results from the Mass Accom runs, while (B) and (D) are results from the D_{org} runs. Solid curves are calculated with the base case parameterization; dashed curves and dashed-dotted curves are calculated with the low and high sensitivity case parameterizations, respectively.

increases the NMB of the IEPOX SOA tracers compared to the base case (Table 2). On the contrary, the lower mass

accommodation coefficient (α = 0.001) leads to larger positive NMB values for Sulf_{inorg} and pronounced decreases in NMB

values for 2-MT and MTS (going from positive to negative values). A similar scaling effect is observed for model runs on individual experiments (Table S4). More importantly, the choice of α significantly affects the reactive uptake rate or SOA formation rate, as this term determines the baseline resistance to the mass transfer of IEPOX into the aerosol phase. As shown in the time series plots (Figure S4), the low α value significantly delayed the onset of SOA production. Although this improved the agreement for 2-MT, it worsened the agreement for $Sulf_{inorg}$ and MTS in low IEPOX:Sulf_{inorg} experiments (Figures S2 and S4). For high IEPOX:Sulf_{inorg} the decay of Sulf_{inorg} and the production of IEPOX SOA tracers were severely underpredicted throughout the entire reaction time (Figure S4). Although the modeled IEPOX SOA tracer curves crossed the measured SOA at around 1 h, the predicted curve would continue to increase beyond the duration of the experiment due to the excessive unreacted IEPOX remaining in the gas phase. Unlike Zhang et al.,47 our result shows that the initial reactive uptake is better simulated with an α value of 0.02 when considering overall agreement of the three particulate tracers (i.e., Sulf_{inorg}, 2-MT, and MTS).

Figure 4A,C shows the modeled resistance in the Mass Accom sensitivity runs for the high IEPOX: $Sulf_{inorg}$ experiment (Expt. 3) and the low IEPOX:Sulf_{inorg} experiment (Expt. 5). In the base and High Accom cases, α (blue curves in Figure 4, associated with the second term on the right-hand side of eq 3) governed the reactive uptake only in the beginning, and the crossover with the diffuso-reactive resistance (pink curves in Figure 4, associated with the third term on the right-hand side of eq 3) occurs near 20 and 10 min with regard to the base and High Accom cases for the high IEPOX:Sulfinorg experiment, respectively. After the crossover, the diffuso-reactive term gains dominance in regulating the reactive uptake. In the Low Accom case, the diffuso-reactive resistance evolves much slower and is at least an order of magnitude smaller than the α resistance throughout. It is also worth noting that the diffuso-reactive term evolves slower in the low $\operatorname{IEPOX:Sulf}_{\operatorname{inorg}}$ experiment than in the high IEPOX:Sulf_{inorg} experiment. This indicates that the selflimiting effect would be less pronounced in low IEPOX:Sulf_{inorg} conditions. In all cases, the resistance associated with the gasphase diffusion (gray curves in Figure 4, associated with the first term on the right-hand side of eq 3) was negligible and barely changed. The resistance analysis suggests that a constant low mass accommodation coefficient ($\alpha = 0.001$) would leave the model insensitive to diffuso-reactive resistance evolution (i.e., self-limiting effect), which negates the effects of core-shell parameterization. The higher the value of α , the more reactive uptake will be controlled by the resistance induced by the

Diffusivity of IEPOX in the Organic Shell. The $D_{\rm org}$ (2 × $10^{-12}\,{\rm cm}^2\,{\rm s}^{-1}$) selected as our base case was based on the work of Zhang et al. The RH condition of their experiments (50–60%) were close to ours (~50%). Two orders of magnitude were chosen as the uncertainty range, given that the measured viscosity also typically has an uncertainty range of at least 2 orders of magnitude. In reality, at a given RH, $D_{\rm org}$ is dependent on the organic shell composition and subject to change over time as the composition evolves, particularly in the presence of OSs. Therefore, we estimated the range of $D_{\rm org}$ from viscosity, calculated using the Vogel–Tammann–Fulcher (VTF) equation based on the glass transition temperature of the organic–water mixture with the observed chemical speciation, as detailed in Section S2.2 and in our previous

work. We do not expect that neglecting $D_{\rm org}$ changes in our model will have a large impact on IEPOX reactive uptake. The calculation above justified the prescription of a constant $D_{\rm org}$ (10 m) rescription of a constant $D_{\rm org}$ (2 m) reactive uptake. The calculation above justified the prescription of a constant $D_{\rm org}$ in our model runs.

Similar to Mass Accom, $D_{\rm org}$ also has pronounced effects on IEPOX SOA formation (Figures 3 and S2). A higher D_{org} results in faster diffusion of IEPOX within the organic shell and, therefore, faster production of both 2-MT and MTS. Conversely, a lower D_{org} would slow down the diffusion and reaction of IEPOX. As mentioned earlier, 2-MT was the most poorly predicted IEPOX SOA tracer in the base case parameterization (NMB = 0.58). The Low D_{org} case resulted in the best model performance (Tables 2 and S7). It greatly reduced the NMB of 2-MT from 0.58 to 0.08 and that of MTS from 0.14 to -0.16. The $Sulf_{inorg}$ performance was not significantly affected by the D_{org} range probed in our study. However, a dependence of the model performance on IEPOX:Sulf_{inorg} is evident. Model performances of Sulf_{inorg} and MTS were more sensitive to the variation in D_{org} for high IEPOX:Sulf_{inorg} experiments (Figure S2 and Table S6). The overall model performance for the High $D_{\rm org}$ case and the High Accom case is similar (Tables 2, S4, and S7). As shown in Figure 4A,C, the initial smaller resistance for the High Accom case leads to slightly faster SOA growth in the beginning (Figure S4). Faster SOA growth, in turn, caused steeper increase in the diffuso-reactive resistance (pink dashed-dotted lines in Figure 4A,C). For the High $D_{\rm org}$ case with the base case mass accommodation ($\alpha = 0.02$), the initial resistance (green curve) was already high, which led to slower initial SOA growth (slower thickening of the organic coating) and, therefore, a more gradual increase in the diffuso-reactive resistance (Figure 4B,D). Overall, the impact of D_{org} is evolving over time since it is within the diffuso-reactive term, which adds additional resistance to the baseline resistance $(1/\alpha)$. Therefore, the extent of this time-dependent self-limiting effect will be dependent on the relative magnitude of the selected α value. Use Figure 4 for visual assistance. For the base case mass accommodation coefficient ($\alpha = 0.02$), the model would be insensitive to a $D_{\rm org} \ge 2 \times 10^{-11} \ {\rm cm^2 \ s^{-1}}$, as shown in Figure 4B,D, even at high IEPOX:Sulf_{inorg} conditions. Similarly in the case of Low Mass Accom, the model would be insensitive to a $D_{\rm org} \ge 2 \times 10^{-12} \, {\rm cm}^2 \, {\rm s}^{-1}$, and the SOA growth will be slow from the beginning to the end. On the other hand, if we pair a low $D_{
m org}$ $(D_{\text{org}} = 2 \times 10^{-13} \text{ cm}^2 \text{ s}^{-1})$ with a high α (0.1), D_{org} would start to dominate the resistance after the first few minutes. However, its development takes time and only catches up with the resistance of the low α later. Thus, the initial growth would be faster than in the case of pairing a high D_{org} with a low α .

Branching Ratios between 2-MT and MTS. The two sensitivity parameters discussed above change the 2-MT and MTS model performance in the same direction. On the other hand, the relative reaction rate constants forming 2-MT and MTS are expected to change the branching ratios of these two products. The literature values reported for nucleophilic reactions of IEPOX are summarized in Table S2. The third-

order nucleophilic reaction rate constants of IEPOX with H₂O and SO_4^{2-} in the literature are typically on the order of 10^{-4} , $^{27-29}$ except for those reported by Piletic et al., 30 whose predictions are 2 and 3 orders of magnitude higher than the others for 2-MT and MTS, respectively. In our calculations, the heterogeneous reaction rate (k_{het}) was still the rate-limiting reaction step compared to the condensed-phase reaction rate (k_{aq}) , even when all of the condensed-phase reaction rate constants were lowered by at least 2 orders of magnitude (Figure S6). Thus, the relative rates between 2-MT and MTS are more important than the absolute rates in our case. The rate constants reported by Piletic et al. favor MTS formation over 2-MT formation $(k_{\text{MT}}/k_{\text{MTS}} = 0.1)$.³⁰ This means MTS would form 10 times faster than 2-MT given equivalent nucleophile concentrations ($[SO_4^{2-}] = [H_2O]$). In contrast, bulk solution measurements made by Eddingsaas et al.²⁷ reported the largest ratio $(k_{\text{MT}}/k_{\text{MTS}} = 5)$, followed by previous work²⁹ that suggested a value of ~0.7, favoring 2-MT formation over MTS.

As expected, changing the $k_{\rm MT}/k_{\rm MTS}$ ratio drastically changed the branching ratios between 2-MT and MTS in the $k_{\rm MT}/k_{\rm MTS}$ sensitivity runs. A low ratio ($k_{\rm MT}/k_{\rm MTS}=0.05$) shifted the modeled branching towards MTS (Tables 2 and S8). A high ratio ($k_{\rm MT}/k_{\rm MTS}=0.2$) favored the production of 2-MT relative to MTS, increasing the overprediction of 2-MT, resulting in the worst model performance for 2-MT of all sensitivity scenarios. However, MTS prediction improved with a very low NMB (-0.04). The predicted Sulf_{inorg} varied inversely with $k_{\rm MT}/k_{\rm MTS}$, and NMB variations (0.01-0.07) between different scenarios were smaller compared to the two IEPOX SOA tracers.

Our analysis demonstrated that $k_{\rm MT}/k_{\rm MTS}$ between 0.05 and 0.1 results in a reasonable prediction of particulate 2-MT-to-MTS branching, while $k_{\rm MT}/k_{\rm MTS} = 0.2$ produces a significant overprediction of particulate 2-MT. All literature-reported thirdorder reaction rate constants, except for those predicted by Piletic et al., lead to an even greater overprediction of particulate 2-MT. As mentioned above in the base case performance, a lower OS branching ratio was observed in runs with higher IEPOX:Sulf_{inorg}, which the base case $k_{\rm MT}/k_{\rm MTS}$ tended to reproduce better than the Low $k_{\rm MT}/k_{\rm MTS}$ case. On the other hand, the Low $k_{\text{MT}}/k_{\text{MTS}}$ case tended to reproduce higher OS branching better in runs with lower IEPOX:Sulf_{inorg}. There are several explanations for this result. First, the current model assumes a constant acidity for the inorganic core. However, in reality, the core may become less acidic due to inorganic-to-OS conversion, as our previous work has shown.³⁴ Assuming constant acidity will likely overpredict the reactions in the core that involve H⁺. Second, [SO₄²⁻]/[HSO₄⁻] will increase as the inorganic core becomes less acidic. Since $SO_4^{\ 2-}$ is the major nucleophile responsible for the formation of MTS, the shift in the equilibrium between SO_4^{2-} and HSO_4^{-} inevitably affects the MTS formation rate. Third, the non-ideality manifested as the deviation of ion activity coefficients from 1 may also change as the composition evolves over time. This complex interplay between the kinetic and thermodynamic effects on the condensed-phase reactions warrants future investigation.

Extreme Time-Dependent Self-Limiting Effect in the High IEPOX:Sulf_{inorg} Condition. From the sensitivity analysis, it appears that the model with the base mass accommodation coefficient (α = 0.02), low diffusion coefficient ($D_{\rm org}$ = 2 × 10⁻¹³ cm² s⁻¹), and a higher OS branching ratio ($k_{\rm MT}/k_{\rm MTS}$ = 0.05 – 0.1) best predicts the evolution of the particulate tracers Sulf_{inorg} 2-MT, and MTS. The modeling assumption of constant sensitivity parameters, however, still fails to capture the initial

faster growth and sudden plateau of SOA growth in the high IEPOX:Sulf_{inorg} experiments (Figures 2A and S4). This could be attributed partially, if not completely, to the rapidly changing aerosol acidity under this condition. As shown in Figure S6, the calculated condensed-phase reaction rate ($k_{\rm aq}$) was decreasing faster than the heterogeneous reaction rate ($k_{\rm het}$) and becoming the limiting step in the second half of the run if [H+] were treated as time-dependent, based on our thermodynamic calculation (Section S2.2). Note that all condensed-phase third-order reaction rate constants were scaled down by 100-fold in Figure S6, showing that the self-limiting acidity effect will be sensitive to the absolute third-order reaction rate constants chosen.

For a test, we replaced the constant acidity assumed in the base case parameterization with a time-dependent [H⁺] trend estimated from the thermodynamic model described in Zhang et al.,34 using measured tracer concentrations as input while keeping other model parameters the same as the base case parameterization. The estimated [H⁺] trend was then interpolated inline at each time step during the simulation. The resulting time series of simulated IEPOX SOA tracers and the [H⁺] evolution for the high (Expt. 3) and low (Expt. 5) IEPOX:Sulf_{inorg} experiments are shown in Figure S7. For the high IEPOX: $\check{\text{Sulf}}_{\text{inorg}}$ experiment, the prediction of 2-MT and MTS was improved, especially for the second half of the experiment. The decay of Sulf_{inorg} is slightly slower than the base case parameterization (Figure S7A,C). The MTS dimer, however, is greatly enhanced due to the slower formation of MTS and leads to an overestimation of SOA in the second half of the experiment. For the low $\text{IEPOX:Sulf}_{\text{inorg}}$ experiment, the model performance was marginally the same as the base case owing to smaller changes in the core and shell acidity (Figure S7B,D). The production of dimers in this case was comparable to that in the high IEPOX: $Sulf_{\rm inorg}$ experiment.

The sensitivity test above highlights the importance of considering the thermodynamic effect, especially when IEPOX is in great excess compared to the Sulf_{inorg} aerosol. Notably, the current thermodynamic calculation adapted from Zhang et al. assumes constant activity coefficients for all ionic species and a pK_a of 2 for OSs.³⁴ Our pK_a assumption for OSs was supported by Raman spectroscopy determination using authentic 2-MTS standards, suggesting a p K_a between 2 and 3.69 Another recent bulk solution measurement shows that the dominant tertiary MTS has a pK_a of 2.9–3.1 and depends on the stereochemistry. We tested a pK_a of 3 for OSs using the thermodynamic model from Zhang et al. and found no change in the predicted shell and core acidities compared to using a p K_a of 2 for OSs. Another observation is the unrealistic production of oligomeric OSs. Although the oligomers were not quantified in the current study due to the lack of authentic standards and low intensities detected in the PILS-HILIC/ESI-HR-QTOFMS samples, the mass balance between the sum of monomers (2-MT + MTS) and the total SOA mass estimated from the SEMS shows a marginal difference. This is consistent with our previous work reporting that 2-MT and MTS together contribute >90% of the trans-β-IEPOX SOA mass. 19 A hypothetical loss of oligomeric OSs to volatile species with a $\tau \sim 0.3$ h would lower the production of oligomers and result in better total SOA agreement (Figure S8). The stability of IEPOX-derived oligomers and potential decomposition to volatile species are unknown and warrant future studies.

Other Uncertainties. Recent work by Frauenheim et al. combining chamber experiments and synthesis of standards sheds new insights into the debate over the reactive uptake

products of IEPOX $(C_5H_{10}O_3)$ resulting from acid-driven isomerization in the condensed phase. In that study, Frauenheim et al. synthesized C₅H₁₀O₃ candidates (3methyltetrahydrofuran-2,4-diols and 3-methylenebutane-1,2,4triols) and confirmed that they are indeed IEPOX reactive products found in the aerosol particle filters (as well as in the gas phase) of chamber-generated trans- β -IEPOX SOA. Including this pathway that competes with nucleophilic reactions in the model may impact the formation of other IEPOX SOA tracers. Meanwhile, it may not be manifested in the aerosol phase if its volatility is high. Future studies should focus on constraining the condensed-phase reaction kinetics, leading to these more recently characterized C₅H₁₀O₃ reactive uptake products and their volatilities. Such areas of focus could also benefit if simultaneous real-time gas-phase measurements were made for C₅H₁₀O₃ products as well as 2-MT. This will help to further constrain the semivolatile partitioning of 2-MT between the gas and viscous phase-separated aerosol particles.

Real-time IEPOX quantification is lacking in the current study. As described in the Experimental Section, the IEPOX first-order injection rate was varied to match the 1 h injection mass determined by weighing the manifold before and after the injection. In our previous work, the IEPOX injection rate was tuned to match the time scales of SOA growth.²⁹ The analytical balance reading is sensitive to the temperature of the manifold, which creates some possible uncertainty. The injection function also does not account for insufficient heating due to bad contact of the heating tape. These experimental procedures are translated into the uncertainty of the fitted IEPOX injection rate. Taking Expt. 9 as an example, the time series of the base case shows that the onset of growth (~20 min) was delayed compared to normal onset (~10 min) (Figure S4). We suspect that the actual IEPOX injection was not as efficient as usual due to the experimental procedures discussed above. Therefore, the injection rate fitted for this experiment might be faster than usual and, thus, predicted faster consumption of sulfate and formation of SOA. Consistently, the NMBs of 2-MT and MTS increase while the NMB of Sulfinorg moves in the opposite direction (Figure 1). The uncertainty in the model treatment of IEPOX injection can potentially play an important role and partially explain the large NMB variability even for experiments with similar IEPOX:Sulf_{inorg}. Accurate online quantification of IEPOX vapors in future studies could provide further constraints on the model parametrization of IEPOX injection rates.

Resistor model representations of IEPOX reactive uptake typically assumes the same mass accommodation coefficient (α) with and without organic coating. ^{33,34,36,37} As mentioned above, a base value of 0.02 for α best reproduces the measured γ of (1.9 ± 0.1) $\times 10^{-2}$ reported for the acidified ammonium sulfate seed aerosol in our previous flow tube experiments.³² It may be reasonable to use this value for initial IEPOX uptake onto acidified ammonium sulfate aerosol given the short time scales of the flow tube experiments (20–100 s). However, this value may not be suitable for phase-separated particles with semisolid shell and requires further constraint. It is also unknown what the surface structure of the organic coating is like and how surface processes can impact mass accommodation and IEPOX uptake. These remaining uncertainties can be examined in future studies by using different modeling frameworks that are capable of representing the processes in gas-to-surface and surface-to-bulk interfacial regions. 61-66,72,73

Application of the Phase-Separation Model to a Typical Ambient Condition. Ambient concentrations of

ı

IEPOX and Sulf_{inorg} aerosol are much lower than those in the chamber studies. To put our results into context, we applied our phase-separation model to a hypothetical atmospheric condition: 50% RH, ~0.5 ppbv of gas-phase IEPOX, 250 μ m² cm⁻³ of ammonium bisulfate aerosol surface area, corresponding to an aerosol mass loading of ~10 μ g m⁻³, and an average particle diameter of 100 nm. The rate of gas-phase loss of IEPOX to reaction with ⁶OH was estimated to be 1.8 × 10⁻¹¹ cm³ molecules⁻¹ s^{-113,74} and [⁶OH] = 1.5 × 10⁶ molecules cm^{-3,75} Figure 5 shows the model output using the base case model

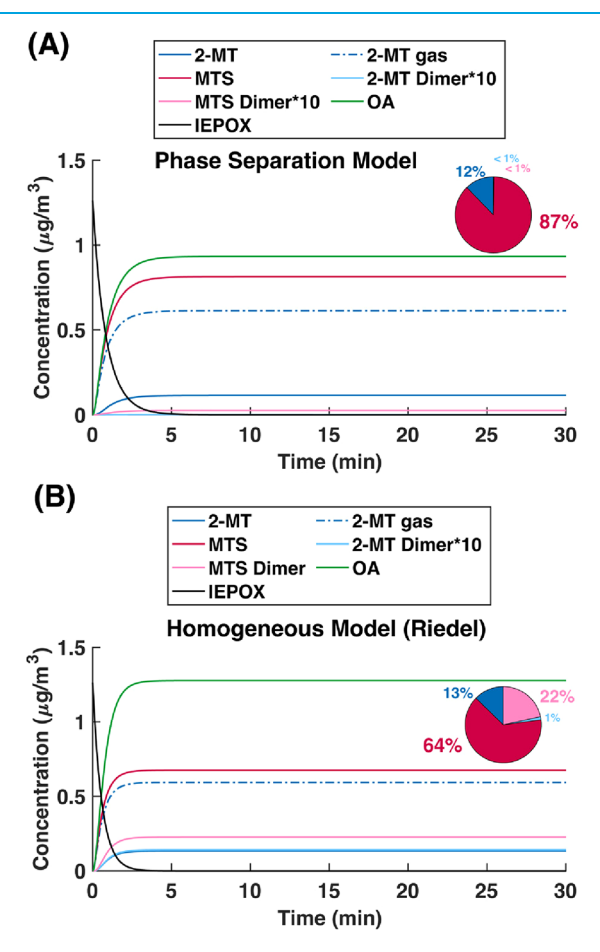


Figure 5. Simulation results for IEPOX reactive uptake under atmospheric relevant conditions (low IEPOX:Sulf_{inorg}). (A) Phase-separation model with base case model parameters except that all third-order reaction rate constants are scaled down by 100-fold. (B) Homogeneous model (Riedel Model) with the same third-order reaction rate constants used in (A).

parameters with third-order reaction rate constants scaled down by 100-fold. As discussed in the previous section, this is necessary for high IEPOX:Sulf_{inorg} chamber experiments to show sensitivity to the self-limiting parameterization. Unlike modeling of the chamber experiments, vapor and particle wall loss for the hypothetical atmospheric aerosol model run was set to zero, and [IEPOX] was set to 0.5 ppbv at t=0. The phase-separation model predicted 0.93 μ g m⁻³ of total SOA, with the bulk (87%) being MTS, a minor amount (12%) of 2-MT, and negligible amounts of MTS and 2-MT dimers (<1%). For comparison, we simulated this atmospherically relevant case with our previous model that assumes a homogeneous particle phase and neglects the self-limiting effect.²⁹ We did, however, allow for 2-MT off-gassing, which was not included in the

original model. The homogeneous-phase model (Riedel Model) with the same third-order reaction rate constants predicted 38% more total SOA formation (1.28 μ g m⁻³) than the phaseseparation model. The MTS dimer contribution was greatly enhanced (22%) and, in turn, the MTS monomer contribution to total SOA was reduced (64%). 2-MT remained a minor branching reaction (13%) in this case. We also tested the Riedel Model with the third-order reaction rate constants reported in the original publication (Table S2). The reactions forming C_5 alkene triols and 3-MeTHF-3,4-diols were turned off. Consistent with the results of Riedel et al., the rate constants favored the formation of 2-MT over MTS (Figure S9). By treating 2-MT as semivolatile ($C^* = 8.31 \,\mu\text{g m}^{-3}$), it resulted in more 2-MT partitioning to the gas phase at such a low SOA mass loading (\sim 1 μ g m⁻³), leading to an overall lower total SOA mass loading (0.81 μg m⁻³). The modeling exercises confirm the importance of considering the self-limiting effect (otherwise, overprediction of SOA is expected) in modeling atmospherically relevant IEPOX SOA formation conditions and the relative rate constants of formation of the two major products (2-MT and MTS).

With the phase-separation model, IEPOX SOA formation was predicted to reach a growth peak within minutes for ammonium bisulfate under the mimic ambient conditions described above (Figure 5A). The salient factors that control the model performance for the chamber conditions, such as α and D_{org} values, have no impact in the final SOA mass and composition formed but delayed the attainment of growth peak by up to 1 h (Figure S10). In contrast, a much longer processing time (\sim 3 h) is required for a hypothetical high IEPOX:Sulf_{inorg} ambient case (~1 ppbv IEPOX and ~0.1 μ g m⁻³ ammonium bisulfate) to reach a growth peak (Figure S11A). The predicted total SOA was dominated by MTS (81%) as even more 2-MT would be present in the gas phase, given the lower SOA mass loading ($\sim 0.3 \ \mu g \ m^{-3}$). The MTS dimer contribution increased from <1% to 8% in this case. Accurately representing the oligomerization kinetics relies on better constraints on both the shell acidity prediction and the reaction rate constants of oligomer formation. The monomer contribution will be affected by changes in the oligomerization rates. It remains challenging, as authentic standards for IEPOX-derived oligomers are lacking. Lowering α and D_{org} significantly slows the reactive uptake processing despite producing similar SOA mass (Figure S11C,D). Nonetheless, MTS should make up the bulk of the $IEPOX-derived \ SOA \ in \ high \ IEPOX: Sulf_{inorg} \ atmospheric \ cases.$ Note that the 2-MT/MTS branching predicted by our phaseseparation model for the atmospheric cases is consistent with measurements in the southeastern U.S. and Amazon region. An analysis of ambient PM_{2.5} samples for IEPOX SOA tracers shows that particulate MTS dominates over particulate 2-MT at Look Rock, Tennessee, U.S., in summer 2013 (2.33 versus 0.86 μ g m⁻³) and at Manaus, Brazil in the transition of dry-to-wet season in 2016 (0.390 versus 0.137 μ g m⁻³).

In summary, a phase-separation model is suited to reflecting the self-limiting IEPOX reactive uptake. Recommended values for key parameters using the phase-separation representation are summarized in Table 3. Our analysis shows that a $k_{\rm MT}/k_{\rm MTS}$ lower than 0.1 is necessary to reflect the ratio of key products. The absolute order of magnitude of the rate constants is important when we apply the phase-separation parametrization to conditions with high IEPOX:Sulf_{inorg} values. Therefore, we recommend Piletic rate constants scaled down by 100-fold for 2-MT and MTS $(5.3\times10^{-4}$ and 5.2×10^{-3} ${\rm M}^{-2}$ s $^{-1})$. The

Table 3. Recommendations on Key Core—Shell Parameterizations

name	parameter	values for consideration
mass accommodation coefficient	α	$0.02 - 0.1^a$
IEPOX organic-phase diffusion coefficient $(cm^2 s^{-1})$	$D_{ m org}$	$2 \times 10^{-13} \text{ at}$ RH ~ $50\%^{b}$
third-order reaction rate constant of IEPOX with $SO_4^{2-}(M^{-2}\ s^{-1})$	$k_{\mathrm{SO_4}^{2-},\mathrm{IEPOX},\mathrm{H}^+}$	5.2×10^{-3}
ratio of third-order reaction rate constant of IEPOX with water and SO ₄ ²⁻	$k_{ m MT}/k_{ m MTS}$	$0.05 - 0.1^{c,d}$

^aModel was less sensitive to the mass accommodation coefficient in this range, which is needed to reproduce initially fast reactive uptake on inorganic seeds. Caution should be made in using low values. The extremely low number of 0.001 reported by Zhang et al. 47 was likely due to the model treatment of IEPOX injection (see Section S3). b This $D_{
m org}$ results in better model performance in the sensitivity runs and falls in the middle of the estimated D_{org} uncertainty range. However, picking a value an order of magnitude higher or lower than this is not unreasonable, considering that even the measured viscosity has an uncertainty of at least 2 orders of magnitude.⁶⁸ Please note that the model sensitivity to D_{org} will be dependent on $\alpha.$ Avoid picking The lower or higher end of the range for α and $D_{\rm org}$ at the same time. Consider using a dry $T_{\rm gorg}$ of 255 °C to calculate $D_{\rm org}$ if extended to other RH conditions. If acidity is held constant, using the Piletic et al. rate constants or other lower rate constants will not matter too much. If acidity is treated as time-dependent, we recommended tuning down the Piletic et al. rate constants by an order of magnitude (table value). A lower rate constant will make the model more sensitive to timedependent acidity. ^dPick a lower ratio (strongly favoring MTS) for low IEPOX:Sulf_{inorg} conditions and a higher ratio (intermediately favoring MTS) for high IEPOX:Sulfinorg.

sensitivity parameters α and D_{org} are important to predicting the time that it takes for IEPOX reactive uptake to plateau. The time it takes to reach the growth peak is an important consideration, particularly for high IEPOX:Sulfinorg conditions, where the model predicts it takes several hours to reach the growth peak. Several hours are not negligible when the regional and climate models are dealing with a time scale of minutes to hours. A value of 0.02 is recommended for α according to the sensitivity analysis of the results from chamber experiments. For D_{org} , a constant value of $2 \times 10^{-13} \, \text{cm}^2 \, \text{s}^{-1}$, an order of magnitude lower than that derived from measured composition, results in better observation-model agreement at ~50% RH. This parametric value does not necessarily represent the actual diffusivity. Note that the resistor equations (eqs 3 and 5) contain the product $H_{\rm org}D_{\rm org}$, and based on our sensitivity simulations, 4×10^{-7} M atm $^{-1}$ cm 2 s $^{-1}$ is recommended for $H_{\rm org}D_{\rm org}$ at $\sim 50\%$ RH. Extending the result to other RH values is possible given the dependence of viscosity on RH, although caution needs to be taken. Octaviani et al. has shown that $H_{\rm org}D_{\rm org}$ derived via such an approach would completely halt the uptake under dry conditions (<5% RH), contrary to the observation.⁴⁶ This suggests a need to validate the assumption of a constant H_{org} with different chemical composition and RH. Future experiments targeting low levels of pollutant concentrations under a range of atmospherically relevant RH levels will be beneficial to evaluate the phase-separation model and constrain the sensitivity parameters, including $H_{
m org}$ and $D_{
m org}$

ASSOCIATED CONTENT

Supporting Information

The Supporting Information is available free of charge at https://pubs.acs.org/doi/10.1021/acsestair.4c00002.

Additional experimental and modeling procedures, schematic of IEPOX reactive uptake experiments, NMB of modeled aerosol-phase species as a function of IEPOX:Sulf_{inorg}, scatter plots and time series plots of modeled and observed aerosol-phase species by experiment and modeling scenarios, time series of estimated D_{org} evolution, time series of k_{het} and k_{aq} from base case parameterization, time series plots of modeled and observed aerosol-phase species considering time-dependent acidity and oligomer decomposition, modeled IEPOX SOA under ambient relevant conditions using different models and assumptions, summary of chamber experiments, third-order reaction rate constants from the literature and present work, NMB of modeled aerosolphase species for individual experiments for all modeling scenarios, glass transition temperatures, activity coefficients, and a comparison with previous chamber modeling studies (PDF)

AUTHOR INFORMATION

Corresponding Author

Jason D. Surratt — Department of Environmental Sciences and Engineering, Gillings School of Global Public Health, The University of North Carolina at Chapel Hill, Chapel Hill, North Carolina 27599, United States; orcid.org/0000-0002-6833-1450; Email: surratt@unc.edu

Authors

- Yuzhi Chen Department of Environmental Sciences and Engineering, Gillings School of Global Public Health, The University of North Carolina at Chapel Hill, Chapel Hill, North Carolina 27599, United States; Present Address: Atmospheric, Climate, & Earth Sciences Division, Pacific Northwest National Laboratory, Richland, Washington 99352, United States; orcid.org/0000-0002-2547-8428
- Alexandra E. Ng Department of Environmental Sciences and Engineering, Gillings School of Global Public Health, The University of North Carolina at Chapel Hill, Chapel Hill, North Carolina 27599, United States
- Jaime Green Department of Environmental Sciences and Engineering, Gillings School of Global Public Health, The University of North Carolina at Chapel Hill, Chapel Hill, North Carolina 27599, United States
- Yue Zhang Department of Environmental Sciences and Engineering, Gillings School of Global Public Health, The University of North Carolina at Chapel Hill, Chapel Hill, North Carolina 27599, United States; Department of Atmospheric Sciences, Texas A&M University, College Station, Texas 77843, United States
- Matthieu Riva Univ Lyon, Université Claude Bernard Lyon 1, CNRS, IRCELYON, Villeurbanne 69626, France; orcid.org/0000-0003-0054-4131
- Theran P. Riedel Office of Research and Development, U.S. Environmental Protection Agency, Research Triangle Park, North Carolina 27711, United States; orcid.org/0000-0001-5094-4892
- Havala O. T. Pye Office of Research and Development, U.S. Environmental Protection Agency, Research Triangle Park, North Carolina 27711, United States; orcid.org/0000-0002-2014-2140
- Ziying Lei Department of Environmental Health Sciences, University of Michigan, Ann Arbor, Michigan 48109, United

- States; Present Address: Department of Atmospheric Science, Texas A&M University, College Station, Texas 77843, United States
- Nicole E. Olson Department of Chemistry, University of Michigan, Ann Arbor, Michigan 48109, United States;
 Present Address: Office of Research and Development, U.S. Environmental Protection Agency, Research Triangle Park, North Carolina 27711, United States
- Madeline E. Cooke Department of Chemistry, University of Michigan, Ann Arbor, Michigan 48109, United States
- Zhenfa Zhang Department of Environmental Sciences and Engineering, Gillings School of Global Public Health, The University of North Carolina at Chapel Hill, Chapel Hill, North Carolina 27599, United States
- William Vizuete Department of Environmental Sciences and Engineering, Gillings School of Global Public Health, The University of North Carolina at Chapel Hill, Chapel Hill, North Carolina 27599, United States
- Avram Gold Department of Environmental Sciences and Engineering, Gillings School of Global Public Health, The University of North Carolina at Chapel Hill, Chapel Hill, North Carolina 27599, United States; orcid.org/0000-0003-1383-6635
- Barbara J. Turpin Department of Environmental Sciences and Engineering, Gillings School of Global Public Health, The University of North Carolina at Chapel Hill, Chapel Hill, North Carolina 27599, United States; orcid.org/0000-0003-4513-4187
- Andrew P. Ault Department of Chemistry, University of Michigan, Ann Arbor, Michigan 48109, United States; orcid.org/0000-0002-7313-8559

Complete contact information is available at: https://pubs.acs.org/10.1021/acsestair.4c00002

Author Contributions

J.D.S. and A.P.A. conceived of the project, secured funding, and guided the chamber experiments. Y.C. helped design the chamber experiments and developed the phase-separation model with the help of T.P.R. and Y.Z. Z.L. and M.E.C. helped conduct the chamber experiments. Y.C., A.E.N., and J.G. performed the sensitivity analysis. Z.Z. and A.G. synthesized the standards used in performing the chamber experiments and quantifying SOA tracers. The manuscript was written by all authors. All authors have given approval to the final version of the manuscript.

Funding

This work was primarily funded by the National Science Foundation (NSF) Grants AGS 1703019 (A.P.A.) and 1703535 (J.D.S.). The work was also supported in part by NSF Grants AGS-2039788 (J.D.S.), AGS-2040610 (A.P.A.), AGS-2001027 (A.G. and Y.Z.), AGS-2037697 (W.V.), and CHE-1654149 (A.P.A.). Y.Z. acknowledges support from an NSF Postdoctoral Fellowship (AGS-1524731). M.E.C. acknowledges support from an NSF Graduate Research Fellowship (NSF-GRFP) DGE-1841052.

Notes

The contents of this publication are solely the responsibility of the authors and do not necessarily represent the official views of the U.S. Environmental Protection Agency (U.S. EPA). Further, the U.S. EPA does not endorse the purchase of any commercial products or services mentioned in the publication. This work was supported in part by the U.S. Environmental Protection

Agency Office of Research and Development. The views expressed in this article are those of the authors and do not necessarily reflect the views or polices of the U.S. EPA. The authors declare no competing financial interest.

ACKNOWLEDGMENTS

RPLC and HILIC/ESI-HR-QTOFMS work was performed in the UNC Biomarker Mass Spectrometry Facility, which is supported by the National Institute of Environmental Health Sciences (Grant P30ES010126). The authors would like to thank the facility staff members Dr. Leonard B. Collins and Wanda B. Bodnar for their assistance.

ADDITIONAL NOTE

^aT.P.R. passed away on March 12, 2021.

REFERENCES

- (1) Harley, P. C.; Monson, R. K.; Lerdau, M. T. Ecological and Evolutionary Aspects of Isoprene Emission from Plants. *Oecologia* **1999**, *118* (2), 109–123.
- (2) Guenther, A.; Karl, T.; Harley, P.; Wiedinmyer, C.; Palmer, P. I.; Geron, C. Estimates of Global Terrestrial Isoprene Emissions Using MEGAN (Model of Emissions of Gases and Aerosols from Nature). *Atmos. Chem. Phys.* **2006**, *6* (11), 3181–3210.
- (3) Guenther, A. B.; Jiang, X.; Heald, C. L.; Sakulyanontvittaya, T.; Duhl, T.; Emmons, L. K.; Wang, X. The Model of Emissions of Gases and Aerosols from Nature Version 2.1 (MEGAN2.1): An Extended and Updated Framework for Modeling Biogenic Emissions. *Geosci. Model Dev.* 2012, 5 (6), 1471–1492.
- (4) Wennberg, P. O.; Bates, K. H.; Crounse, J. D.; Dodson, L. G.; McVay, R. C.; Mertens, L. A.; Nguyen, T. B.; Praske, E.; Schwantes, R. H.; Smarte, M. D.; St Clair, J. M.; Teng, A. P.; Zhang, X.; Seinfeld, J. H. Gas-Phase Reactions of Isoprene and Its Major Oxidation Products. *Chem. Rev.* **2018**, *118* (7), 3337–3390.
- (5) Paulot, F.; Henze, D. K.; Wennberg, P. O. Impact of the Isoprene Photochemical Cascade on Tropical Ozone. *Atmos. Chem. Phys.* **2012**, 12 (3), 1307–1325.
- (6) Teng, A. P.; Crounse, J. D.; Wennberg, P. O. Isoprene Peroxy Radical Dynamics. J. Am. Chem. Soc. 2017, 139 (15), 5367–5377.
- (7) Kroll, J. H.; Ng, N. L.; Murphy, S. M.; Flagan, R. C.; Seinfeld, J. H. Secondary Organic Aerosol Formation from Isoprene Photooxidation. *Environ. Sci. Technol.* **2006**, 40 (6), 1869–1877.
- (8) Surratt, J. D.; Murphy, S. M.; Kroll, J. H.; Ng, N. L.; Hildebrandt, L.; Sorooshian, A.; Szmigielski, R.; Vermeylen, R.; Maenhaut, W.; Claeys, M.; Flagan, R. C.; Seinfeld, J. H. Chemical Composition of Secondary Organic Aerosol Formed from the Photooxidation of Isoprene. *J. Phys. Chem. A* **2006**, *110* (31), 9665–9690.
- (9) Carlton, A. G.; Wiedinmyer, C.; Kroll, J. H. A Review of Secondary Organic Aerosol (SOA) Formation from Isoprene. *Atmospheric Chemistry and Physics* **2009**, *9* (14), 4987–5005.
- (10) Liu, Y. J.; Herdlinger-Blatt, I.; McKinney, K. A.; Martin, S. T. Production of Methyl Vinyl Ketone and Methacrolein via the Hydroperoxyl Pathway of Isoprene Oxidation. *Atmos. Chem. Phys.* **2013**, *13* (11), 5715–5730.
- (11) Paulot, F.; Crounse, J. D.; Kjaergaard, H. G.; Kürten, A.; St Clair, J. M.; Seinfeld, J. H.; Wennberg, P. O. Unexpected Epoxide Formation in the Gas-Phase Photooxidation of Isoprene. *Science* **2009**, 325 (5941), 730–733.
- (12) St Clair, J. M.; Rivera-Rios, J. C.; Crounse, J. D.; Knap, H. C.; Bates, K. H.; Teng, A. P.; Jørgensen, S.; Kjaergaard, H. G.; Keutsch, F. N.; Wennberg, P. O. Kinetics and Products of the Reaction of the First-Generation Isoprene Hydroxy Hydroperoxide (ISOPOOH) with OH. *J. Phys. Chem. A* **2016**, *120* (9), 1441–1451.
- (13) Bates, K. H.; Crounse, J. D.; St Clair, J. M.; Bennett, N. B.; Nguyen, T. B.; Seinfeld, J. H.; Stoltz, B. M.; Wennberg, P. O. Gas Phase Production and Loss of Isoprene Epoxydiols. *J. Phys. Chem. A* **2014**, *118* (7), 1237–1246.

- (14) Jacobs, M. I.; Burke, W. J.; Elrod, M. J. Kinetics of the Reactions of Isoprene-Derived Hydroxynitrates: Gas Phase Epoxide Formation and Solution Phase Hydrolysis. *Atmos. Chem. Phys.* **2014**, *14* (17), 8933–8946.
- (15) Surratt, J. D.; Kroll, J. H.; Kleindienst, T. E.; Edney, E. O.; Claeys, M.; Sorooshian, A.; Ng, N. L.; Offenberg, J. H.; Lewandowski, M.; Jaoui, M.; Flagan, R. C.; Seinfeld, J. H. Evidence for Organosulfates in Secondary Organic Aerosol. *Environ. Sci. Technol.* **2007**, *41* (2), 517–527.
- (16) Surratt, J. D.; Chan, A. W. H.; Eddingsaas, N. C.; Chan, M.; Loza, C. L.; Kwan, A. J.; Hersey, S. P.; Flagan, R. C.; Wennberg, P. O.; Seinfeld, J. H. Reactive Intermediates Revealed in Secondary Organic Aerosol Formation from Isoprene. *Proc. Natl. Acad. Sci. U. S. A.* **2010**, 107 (15), 6640–6645.
- (17) Lin, Y.-H.; Zhang, Z.; Docherty, K. S.; Zhang, H.; Budisulistiorini, S. H.; Rubitschun, C. L.; Shaw, S. L.; Knipping, E. M.; Edgerton, E. S.; Kleindienst, T. E.; Gold, A.; Surratt, J. D. Isoprene Epoxydiols as Precursors to Secondary Organic Aerosol Formation: Acid-Catalyzed Reactive Uptake Studies with Authentic Compounds. *Environ. Sci. Technol.* **2012**, *46* (1), 250–258.
- (18) Riva, M.; Chen, Y.; Zhang, Y.; Lei, Z.; Olson, N. E.; Boyer, H. C.; Narayan, S.; Yee, L. D.; Green, H. S.; Cui, T.; Zhang, Z.; Baumann, K.; Fort, M.; Edgerton, E.; Budisulistiorini, S. H.; Rose, C. A.; Ribeiro, I. O.; e Oliveira, R. L.; dos Santos, E. O.; Machado, C. M. D.; Szopa, S.; Zhao, Y.; Alves, E. G.; de Sá, S. S.; Hu, W.; Knipping, E. M.; Shaw, S. L.; Duvoisin Junior, S.; de Souza, R. A. F.; Palm, B. B.; Jimenez, J.-L.; Glasius, M.; Goldstein, A. H.; Pye, H. O. T.; Gold, A.; Turpin, B. J.; Vizuete, W.; Martin, S. T.; Thornton, J. A.; Dutcher, C. S.; Ault, A. P.; Surratt, J. D. Increasing Isoprene Epoxydiol-to-Inorganic Sulfate Aerosol Ratio Results in Extensive Conversion of Inorganic Sulfate to Organosulfur Forms: Implications for Aerosol Physicochemical Properties. *Environ. Sci. Technol.* **2019**, *53* (15), 8682–8694.
- (19) Cui, T.; Zeng, Z.; dos Santos, E. O.; Zhang, Z.; Chen, Y.; Zhang, Y.; Rose, C. A.; Budisulistiorini, S. H.; Collins, L. B.; Bodnar, W. M.; dSouza, R. A. F.; Martin, S. T.; Machado, C. M. D.; Turpin, B. J.; Gold, A.; Ault, A. P.; Surratt, J. D. Development of a Hydrophilic Interaction Liquid Chromatography (HILIC) Method for the Chemical Characterization of Water-Soluble Isoprene Epoxydiol (IEPOX)-Derived Secondary Organic Aerosol. *Environ. Sci.: Process. Impacts* **2018**, *20* (11), 1524–1536.
- (20) Hettiyadura, A. P. S.; Al-Naiema, I. M.; Hughes, D. D.; Fang, T.; Stone, E. A. Organosulfates in Atlanta, Georgia: Anthropogenic Influences on Biogenic Secondary Organic Aerosol Formation. *Atmos. Chem. Phys.* **2019**, *19* (5), 3191–3206.
- (21) Glasius, M.; Bering, M. S.; Yee, L. D.; de Sá, S. S.; Isaacman-VanWertz, G.; Wernis, R. A.; Barbosa, H. M. J.; Alexander, M. L.; Palm, B. B.; Hu, W.; Campuzano-Jost, P.; Day, D. A.; Jimenez, J. L.; Shrivastava, M.; Martin, S. T.; Goldstein, A. H. Organosulfates in Aerosols Downwind of an Urban Region in Central Amazon. *Environ. Sci.: Process. Impacts* **2018**, 20 (11), 1546–1558.
- (22) Hughes, D. D.; Christiansen, M. B.; Milani, A.; Vermeuel, M. P.; Novak, G. A.; Alwe, H. D.; Dickens, A. F.; Pierce, R. B.; Millet, D. B.; Bertram, T. H.; Stanier, C. O.; Stone, E. A. PM2.5 Chemistry, Organosulfates, and Secondary Organic Aerosol during the 2017 Lake Michigan Ozone Study. *Atmos. Environ.* 2021, 244, 117939.
- (23) Hu, W. W.; Campuzano-Jost, P.; Palm, B. B.; Day, D. A.; Ortega, A. M.; Hayes, P. L.; Krechmer, J. E.; Chen, Q.; Kuwata, M.; Liu, Y. J.; de Sá, S. S.; McKinney, K.; Martin, S. T.; Hu, M.; Budisulistiorini, S. H.; Riva, M.; Surratt, J. D.; Sclair, J. M.; Isaacman-VanWertz, G.; Yee, L. D.; Goldstein, A. H.; Carbone, S.; Brito, J.; Artaxo, P.; de Gouw, J. A.; Koss, A.; Wisthaler, A.; Mikoviny, T.; Karl, T.; Kaser, L.; Jud, W.; Hansel, A.; Docherty, K. S.; Alexander, M. L.; Robinson, N. H.; Coe, H.; Allan, J. D.; Canagaratna, M. R.; Paulot, F.; Jimenez, J. L. Characterization of a Real-Time Tracer for Isoprene Epoxydiols-Derived Secondary Organic Aerosol (IEPOX-SOA) from Aerosol Mass Spectrometer Measurements. *Atmos. Chem. Phys.* **2015**, *15* (20), 11807–11833.
- (24) Lopez-Hilfiker, F. D.; Iyer, S.; Mohr, C.; Lee, B. H.; D'Ambro, E. L.; Kurtén, T.; Thornton, J. A. Constraining the Sensitivity of Iodide

- Adduct Chemical Ionization Mass Spectrometry to Multifunctional Organic Molecules Using the Collision Limit and Thermodynamic Stability of Iodide Ion Adducts. *Atmospheric Measurement Techniques* **2016**, 9 (4), 1505–1512.
- (25) Budisulistiorini, S. H.; Canagaratna, M. R.; Croteau, P. L.; Marth, W. J.; Baumann, K.; Edgerton, E. S.; Shaw, S. L.; Knipping, E. M.; Worsnop, D. R.; Jayne, J. T.; Gold, A.; Surratt, J. D. Real-Time Continuous Characterization of Secondary Organic Aerosol Derived from Isoprene Epoxydiols in Downtown Atlanta, Georgia, Using the Aerodyne Aerosol Chemical Speciation Monitor. *Environ. Sci. Technol.* 2013, 47 (11), 5686–5694.
- (26) Budisulistiorini, S. H.; Li, X.; Bairai, S. T.; Renfro, J.; Liu, Y.; Liu, Y. J.; McKinney, K. A.; Martin, S. T.; McNeill, V. F.; Pye, H. O. T.; Nenes, A.; Neff, M. E.; Stone, E. A.; Mueller, S.; Knote, C.; Shaw, S. L.; Zhang, Z.; Gold, A.; Surratt, J. D. Examining the Effects of Anthropogenic Emissions on Isoprene-Derived Secondary Organic Aerosol Formation during the 2013 Southern Oxidant and Aerosol Study (SOAS) at the Look Rock, Tennessee Ground Site. *Atmos. Chem. Phys.* 2015, 15 (15), 8871–8888.
- (27) Eddingsaas, N. C.; VanderVelde, D. G.; Wennberg, P. O. Kinetics and Products of the Acid-Catalyzed Ring-Opening of Atmospherically Relevant Butyl Epoxy Alcohols. *J. Phys. Chem. A* **2010**, *114* (31), 8106–8113.
- (28) Cole-Filipiak, N. C.; O'Connor, A. E.; Elrod, M. J. Kinetics of the Hydrolysis of Atmospherically Relevant Isoprene-Derived Hydroxy Epoxides. *Environ. Sci. Technol.* **2010**, *44* (17), 6718–6723.
- (29) Riedel, T. P.; Lin, Y.-H.; Zhang, Z.; Chu, K.; Thornton, J. A.; Vizuete, W.; Gold, A.; Surratt, J. D. Constraining Condensed-Phase Formation Kinetics of Secondary Organic Aerosol Components from Isoprene Epoxydiols. *Atmos. Chem. Phys.* **2016**, *16* (3), 1245–1254.
- (30) Piletic, I. R.; Edney, E. O.; Bartolotti, L. J. A Computational Study of Acid Catalyzed Aerosol Reactions of Atmospherically Relevant Epoxides. *Phys. Chem. Chem. Phys.* **2013**, *15* (41), 18065–18076.
- (31) Gaston, C. J.; Riedel, T. P.; Zhang, Z.; Gold, A.; Surratt, J. D.; Thornton, J. A. Reactive Uptake of an Isoprene-Derived Epoxydiol to Submicron Aerosol Particles. *Environ. Sci. Technol.* **2014**, 48 (19), 11178–11186.
- (32) Riedel, T. P.; Lin, Y.-H.; Budisulistiorini, S. H.; Gaston, C. J.; Thornton, J. A.; Zhang, Z.; Vizuete, W.; Gold, A.; Surratt, J. D. Heterogeneous Reactions of Isoprene-Derived Epoxides: Reaction Probabilities and Molar Secondary Organic Aerosol Yield Estimates. *Environ. Sci. Technol. Lett.* **2015**, 2 (2), 38–42.
- (33) Zhang, Y.; Chen, Y.; Lambe, A. T.; Olson, N. E.; Lei, Z.; Craig, R. L.; Zhang, Z.; Gold, A.; Onasch, T. B.; Jayne, J. T.; Worsnop, D. R.; Gaston, C. J.; Thornton, J. A.; Vizuete, W.; Ault, A. P.; Surratt, J. D. Effect of the Aerosol-Phase State on Secondary Organic Aerosol Formation from the Reactive Uptake of Isoprene-Derived Epoxydiols (IEPOX). *Environ. Sci. Technol. Lett.* **2018**, 5 (3), 167–174.
- (34) Zhang, Y.; Chen, Y.; Lei, Z.; Olson, N. E.; Riva, M.; Koss, A. R.; Zhang, Z.; Gold, A.; Jayne, J. T.; Worsnop, D. R.; Onasch, T. B.; Kroll, J. H.; Turpin, B. J.; Ault, A. P.; Surratt, J. D. Joint Impacts of Acidity and Viscosity on the Formation of Secondary Organic Aerosol from Isoprene Epoxydiols (IEPOX) in Phase Separated Particles. ACS Earth Space Chem. 2019, 3 (12), 2646–2658.
- (35) Budisulistiorini, S. H.; Nenes, A.; Carlton, A. G.; Surratt, J. D.; McNeill, V. F.; Pye, H. O. T. Simulating Aqueous-Phase Isoprene-Epoxydiol (IEPOX) Secondary Organic Aerosol Production During the 2013 Southern Oxidant and Aerosol Study (SOAS). *Environ. Sci. Technol.* **2017**, *51* (9), 5026–5034.
- (36) Schmedding, R.; Rasool, Q. Z.; Zhang, Y.; Pye, H. O. T.; Zhang, H.; Chen, Y.; Surratt, J. D.; Lopez-Hilfiker, F. D.; Thornton, J. A.; Goldstein, A. H.; Vizuete, W. Predicting Secondary Organic Aerosol Phase State and Viscosity and Its Effect on Multiphase Chemistry in a Regional-Scale Air Quality Model. *Atmos. Chem. Phys.* **2020**, *20* (13), 8201–8225.
- (37) Schmedding, R.; Ma, M.; Zhang, Y.; Farrell, S.; Pye, H. O. T.; Chen, Y.; Wang, C.; Rasool, Q. Z.; Budisulistiorini, S. H.; Ault, A. P.; Surratt, J. D.; Vizuete, W. α -Pinene-Derived Organic Coatings on

- Acidic Sulfate Aerosol Impacts Secondary Organic Aerosol Formation from Isoprene in a Box Model. *Atmos. Environ.* **2019**, 213, 456–462.
- (38) Pye, H. O. T.; Pinder, R. W.; Piletic, I. R.; Xie, Y.; Capps, S. L.; Lin, Y.-H.; Surratt, J. D.; Zhang, Z.; Gold, A.; Luecken, D. J.; Hutzell, W. T.; Jaoui, M.; Offenberg, J. H.; Kleindienst, T. E.; Lewandowski, M.; Edney, E. O. Epoxide Pathways Improve Model Predictions of Isoprene Markers and Reveal Key Role of Acidity in Aerosol Formation. *Environ. Sci. Technol.* **2013**, *47* (19), 11056–11064.
- (39) McNeill, V. F.; Woo, J. L.; Kim, D. D.; Schwier, A. N.; Wannell, N. J.; Sumner, A. J.; Barakat, J. M. Aqueous-Phase Secondary Organic Aerosol and Organosulfate Formation in Atmospheric Aerosols: A Modeling Study. *Environ. Sci. Technol.* **2012**, *46* (15), 8075–8081.
- (40) Shrivastava, M.; Andreae, M. O.; Artaxo, P.; Barbosa, H. M. J.; Berg, L. K.; Brito, J.; Ching, J.; Easter, R. C.; Fan, J.; Fast, J. D.; Feng, Z.; Fuentes, J. D.; Glasius, M.; Goldstein, A. H.; Alves, E. G.; Gomes, H.; Gu, D.; Guenther, A.; Jathar, S. H.; Kim, S.; Liu, Y.; Lou, S.; Martin, S. T.; McNeill, V. F.; Medeiros, A.; de Sá, S. S.; Shilling, J. E.; Springston, S. R.; Souza, R. A. F.; Thornton, J. A.; Isaacman-VanWertz, G.; Yee, L. D.; Ynoue, R.; Zaveri, R. A.; Zelenyuk, A.; Zhao, C. Urban Pollution Greatly Enhances Formation of Natural Aerosols over the Amazon Rainforest. *Nat. Commun.* **2019**, *10* (1), 1046.
- (41) Jo, D. S.; Hodzic, A.; Emmons, L. K.; Marais, E. A.; Peng, Z.; Nault, B. A.; Hu, W.; Campuzano-Jost, P.; Jimenez, J. L. A Simplified Parameterization of Isoprene-Epoxydiol-Derived Secondary Organic Aerosol (IEPOX-SOA) for Global Chemistry and Climate Models: A Case Study with GEOS-Chem v11-02-rc. *Geosci. Model Dev.* **2019**, *12* (7), 2983.
- (42) Shrivastava, M.; Cappa, C. D.; Fan, J.; Goldstein, A. H.; Guenther, A. B.; Jimenez, J. L.; Kuang, C.; Laskin, A.; Martin, S. T.; Ng, N. L.; Petaja, T.; Pierce, J. R.; Rasch, P. J.; Roldin, P.; Seinfeld, J. H.; Shilling, J.; Smith, J. N.; Thornton, J. A.; Volkamer, R.; Wang, J.; Worsnop, D. R.; Zaveri, R. A.; Zelenyuk, A.; Zhang, Q. Recent Advances in Understanding Secondary Organic Aerosol: Implications for Global Climate Forcing. *Rev. Geophys.* **2017**, *55* (2), 509–559.
- (43) Lei, Z.; Chen, Y.; Zhang, Y.; Cooke, M. E.; Ledsky, I. R.; Armstrong, N. C.; Olson, N. E.; Zhang, Z.; Gold, A.; Surratt, J. D.; Ault, A. P. Initial pH Governs Secondary Organic Aerosol Phase State and Morphology after Uptake of Isoprene Epoxydiols (IEPOX). *Environ. Sci. Technol.* **2022**, *56* (15), 10596–10607.
- (44) Olson, N. E.; Lei, Z.; Craig, R. L.; Zhang, Y.; Chen, Y.; Lambe, A. T.; Zhang, Z.; Gold, A.; Surratt, J. D.; Ault, A. P. Reactive Uptake of Isoprene Epoxydiols Increases the Viscosity of the Core of Phase-Separated Aerosol Particles. *ACS Earth Space Chem.* **2019**, *3* (8), 1402–1414
- (45) Shrivastava, M.; Rasool, Q. Z.; Zhao, B.; Octaviani, M.; Zaveri, R. A.; Zelenyuk, A.; Gaudet, B.; Liu, Y.; Shilling, J. E.; Schneider, J.; Schulz, C.; Zöger, M.; Martin, S. T.; Ye, J.; Guenther, A.; Souza, R. F.; Wendisch, M.; Pöschl, U. Tight Coupling of Surface and In-Plant Biochemistry and Convection Governs Key Fine Particulate Components over the Amazon Rainforest. ACS Earth Space Chem. 2022, 6 (2), 380–390.
- (46) Octaviani, M.; Shrivastava, M.; Zaveri, R. A.; Zelenyuk, A.; Zhang, Y.; Rasool, Q. Z.; Bell, D. M.; Riva, M.; Glasius, M.; Surratt, J. D. Modeling the Size Distribution and Chemical Composition of Secondary Organic Aerosols during the Reactive Uptake of Isoprene-Derived Epoxydiols under Low-Humidity Condition. *ACS Earth Space Chem.* **2021**, *5* (11), 3247–3257.
- (47) Zhang, J.; Shrivastava, M.; Zelenyuk, A.; Zaveri, R. A.; Surratt, J. D.; Riva, M.; Bell, D.; Glasius, M. Observationally Constrained Modeling of the Reactive Uptake of Isoprene-Derived Epoxydiols under Elevated Relative Humidity and Varying Acidity of Seed Aerosol Conditions. ACS Earth Space Chem. 2023, 7 (4), 788–799.
- (48) Cooke, M. E.; Armstrong, N. C.; Lei, Z.; Chen, Y.; Waters, C. M.; Zhang, Y.; Buchenau, N. A.; Dibley, M. Q.; Ledsky, I. R.; Szalkowski, T.; Lee, J. Y.; Baumann, K.; Zhang, Z.; Vizuete, W.; Gold, A.; Surratt, J. D.; Ault, A. P. Organosulfate Formation in Proxies for Aged Sea Spray Aerosol: Reactive Uptake of Isoprene Epoxydiols to Acidic Sodium Sulfate. ACS Earth Space Chem. 2022, 6 (12), 2790–2800.

- (49) Watanabe, A. C.; Stropoli, S. J.; Elrod, M. J. Assessing the Potential Mechanisms of Isomerization Reactions of Isoprene Epoxydiols on Secondary Organic Aerosol. *Environ. Sci. Technol.* **2018**, *52* (15), 8346–8354.
- (50) Lopez-Hilfiker, F. D.; Mohr, C.; D'Ambro, E. L.; Lutz, A.; Riedel, T. P.; Gaston, C. J.; Iyer, S.; Zhang, Z.; Gold, A.; Surratt, J. D.; Lee, B. H.; Kurten, T.; Hu, W. W.; Jimenez, J.; Hallquist, M.; Thornton, J. A. Molecular Composition and Volatility of Organic Aerosol in the Southeastern U.S.: Implications for IEPOX Derived SOA. *Environ. Sci. Technol.* **2016**, *50* (5), 2200–2209.
- (51) D'Ambro, E. L.; Schobesberger, S.; Gaston, C. J.; Lopez-Hilfiker, F. D.; Lee, B. H.; Liu, J.; Zelenyuk, A.; Bell, D.; Cappa, C. D.; Helgestad, T.; Li, Z.; Guenther, A.; Wang, J.; Wise, M.; Caylor, R.; Surratt, J. D.; Riedel, T.; Hyttinen, N.; Salo, V.-T.; Hasan, G.; Kurtén, T.; Shilling, J. E.; Thornton, J. A. Chamber-Based Insights into the Factors Controlling IEPOX SOA Yield, Composition, and Volatility. *Atmos. Chem. Phys.* **2019**, *19*, 11253.
- (52) Pye, H. O. T.; Zuend, A.; Fry, J. L.; Isaacman-VanWertz, G.; Capps, S. L.; Appel, K. W.; Foroutan, H.; Xu, L.; Ng, N. L.; Goldstein, A. H. Coupling of Organic and Inorganic Aerosol Systems and the Effect on Gas-Particle Partitioning in the Southeastern US. *Atmos. Chem. Phys.* **2018**, *18* (1), 357–370.
- (53) Anttila, T.; Kiendler-scharr, A.; Tillmann, R.; Mentel, T. F. On the Reactive Uptake of Gaseous Compounds by Organic-Coated Aqueous Aerosols: Theoretical Analysis and Application to the Heterogeneous Hydrolysis of N2O5. *J. Phys. Chem. A* **2006**, *110* (35), 10435–10443.
- (54) Zhang, H.; Surratt, J. D.; Lin, Y. H.; Bapat, J.; Kamens, R. M. Effect of Relative Humidity on SOA Formation from Isoprene/NO Photooxidation: Enhancement of 2-Methylglyceric Acid and Its Corresponding Oligoesters under Dry Conditions. *Atmos. Chem. Phys.* **2011**, *11* (13), 6411–6424.
- (55) Gharagheizi, F.; Eslamimanesh, A.; Mohammadi, A. H.; Richon, D. Representation and Prediction of Molecular Diffusivity of Nonelectrolyte Organic Compounds in Water at Infinite Dilution Using the Artificial Neural Network-Group Contribution Method. *Journal of Chemical & Engineering Data* **2011**, *56* (5), 1741–1750.
- (56) de la Puente, M.; Laage, D. How the Acidity of Water Droplets and Films Is Controlled by the Air-Water Interface. *J. Am. Chem. Soc.* **2023**, *145* (46), 25186–25194.
- (57) Lee, J. K.; Walker, K. L.; Han, H. S.; Kang, J.; Prinz, F. B.; Waymouth, R. M.; Nam, H. G.; Zare, R. N. Spontaneous Generation of Hydrogen Peroxide from Aqueous Microdroplets. *Proc. Natl. Acad. Sci. U. S. A.* **2019**, *116* (39), 19294–19298.
- (58) Wexler, A. S.; Clegg, S. L. Atmospheric Aerosol Models for Systems Including the Ions H+, NH4+, Na+, SO42-, NO3-, Cl-, Br-, and H2O. *J. Geophys. Res.: Atmos.* 2002, 107 (D14), 14-1.
- (59) Clegg, S. L.; Brimblecombe, P.; Wexler, A. S. Thermodynamic Model of the System H+-NH4 +-SO4 2-NO3 -H2O at Tropospheric Temperatures. *J. Phys. Chem. A* **1998**, *102* (12), 2137–2154.
- (60) Seinfeld, J. H.; Pandis, S. N. In Atmospheric Chemistry and Physics: From Air Pollution to Climate Change; Wiley, New York, New York, U.S., 1998
- (61) Pöschl, U.; Rudich, Y.; Ammann, M. Kinetic Model Framework for Aerosol and Cloud Surface Chemistry and Gas-Particle Interactions Part 1: General Equations, Parameters, and Terminology. *Atmos. Chem. Phys.* **2007**, *7* (23), 5989–6023.
- (62) Shiraiwa, M.; Pfrang, C.; Koop, T.; Pöschl, U. Kinetic Multi-Layer Model of Gas-Particle Interactions in Aerosols and Clouds (KM-GAP): Linking Condensation, Evaporation and Chemical Reactions of Organics, Oxidants and Water. *Atmos. Chem. Phys.* **2012**, *12* (5), 2777–2794.
- (63) Zaveri, R. A.; Easter, R. C.; Shilling, J. E.; Seinfeld, J. H. Modeling Kinetic Partitioning of Secondary Organic Aerosol and Size Distribution Dynamics: Representing Effects of Volatility, Phase State, and Particle-Phase Reaction. *Atmos Chem. Phys.* **2014**, *14* (10), 5153–5181.
- (64) Julin, J.; Winkler, P. M.; Donahue, N. M.; Wagner, P. E.; Riipinen, I. Near-Unity Mass Accommodation Coefficient of Organic Molecules

- of Varying Structure. Environ. Sci. Technol. 2014, 48 (20), 12083-12089.
- (65) Julin, J.; Shiraiwa, M.; Miles, R. E. H.; Reid, J. P.; Pöschl, U.; Riipinen, I. Mass Accommodation of Water: Bridging the Gap Between Molecular Dynamics Simulations and Kinetic Condensation Models. *J. Phys. Chem. A* **2013**, *117* (2), 410–420.
- (66) Shiraiwa, M.; Pöschl, U. Mass Accommodation and Gas-Particle Partitioning in Secondary Organic Aerosols: Dependence on Diffusivity, Volatility, Particle-Phase Reactions, and Penetration Depth. Atmos. Chem. Phys. 2021, 21 (3), 1565–1580.
- (67) Kolb, C. E.; Cox, R. A.; Abbatt, J. P. D.; Ammann, M.; Davis, E. J.; Donaldson, D. J.; Garrett, B. C.; George, C.; Griffiths, P. T.; Hanson, D. R.; Kulmala, M.; McFiggans, G.; Pöschl, U.; Riipinen, I.; Rossi, M. J.; Rudich, Y.; Wagner, P. E.; Winkler, P. M.; Worsnop, D. R.; O'Dowd, C. D. An Overview of Current Issues in the Uptake of Atmospheric Trace Gases by Aerosols and Clouds. *Atmos. Chem. Phys.* **2010**, *10* (21), 10561–10605.
- (68) DeRieux, W.-S. W.; Li, Y.; Lin, P.; Laskin, J.; Laskin, A.; Bertram, A. K.; Nizkorodov, S. A.; Shiraiwa, M. Predicting the Glass Transition Temperature and Viscosity of Secondary Organic Material Using Molecular Composition. *Atmospheric Chemistry and Physics* **2018**, *18* (9), 6331–6351.
- (69) Fankhauser, A. M.; Lei, Z.; Daley, K. R.; Xiao, Y.; Zhang, Z.; Gold, A.; Ault, B. S.; Surratt, J. D.; Ault, A. P. Acidity-Dependent Atmospheric Organosulfate Structures and Spectra: Exploration of Protonation State Effects via Raman and Infrared Spectroscopies Combined with Density Functional Theory. *J. Phys. Chem. A* **2022**, *126* (35), 5974–5984.
- (70) Varelas, J. G.; Vega, M. M.; Upshur, M. A.; Geiger, F. M.; Thomson, R. J. Synthesis Enabled Investigations into the Acidity and Stability of Atmospherically-Relevant Isoprene-Derived Organosulfates. ACS Earth Space Chem. 2022, 6 (12), 3090–3100.
- (71) Frauenheim, M.; Offenberg, J.; Zhang, Z.; Surratt, J. D.; Gold, A. The C5-Alkene Triol Conundrum: Structural Characterization and Quantitation of Isoprene-Derived C5H10O3 Reactive Uptake Products. *Environ. Sci. Technol. Lett.* **2022**, *9* (10), 829–836.
- (72) Ammann, M.; Pöschl, U. Kinetic Model Framework for Aerosol and Cloud Surface Chemistry and Gas-Particle Interactions Part 2: Exemplary Practical Applications and Numerical Simulations. *Atmos. Chem. Phys.* **2007**, 7 (23), 6025–6045.
- (73) Kolb, C. E.; Worsnop, D. R. Chemistry and Composition of Atmospheric Aerosol Particles. *Phys. Chem.* **2012**, *63* (1), 471–491.
- (74) Jacobs, M. I.; Darer, A. I.; Elrod, M. J. Rate Constants and Products of the OH Reaction with Isoprene-Derived Epoxides. *Environ. Sci. Technol.* **2013**, 47 (22), 12868–12876.
- (75) Mao, J.; Paulot, F.; Jacob, D. J.; Cohen, R. C.; Crounse, J. D.; Wennberg, P. O.; Keller, C. A.; Hudman, R. C.; Barkley, M. P.; Horowitz, L. W. Ozone and Organic Nitrates over the Eastern United States: Sensitivity to Isoprene Chemistry. *J. Geophys. Res.: Atmos.* **2013**, *118* (19), 11256.
- (76) Nguyen, T. B.; Coggon, M. M.; Bates, K. H.; Zhang, X.; Schwantes, R. H.; Schilling, K. A.; Loza, C. L.; Flagan, R. C.; Wennberg, P. O.; Seinfeld, J. H. Organic Aerosol Formation from the Reactive Uptake of Isoprene Epoxydiols (IEPOX) onto Non-Acidified Inorganic Seeds. *Atmospheric Chemistry and Physics* **2014**, *14* (7), 3497–3510.